The Dissertation Committee for Maria João Brito Moura
certifies that this is the approved version of the following dissertation:

Ripples and Cracks in Graphene

Committee:

Michael Marder, Supervisor

Allan MacDonald, Supervisor

Arno Bohm

Alex Demkov

Rod Ruoff

Maxim Tsoi

Ripples and Cracks in Graphene

by

Maria João Brito Moura, B.S.; M.S.

DISSERTATION

Presented to the Faculty of the Graduate School of

The University of Texas at Austin

in Partial Fulfillment

of the Requirements

for the Degree of

DOCTOR OF PHILOSOPHY

THE UNIVERSITY OF TEXAS AT AUSTIN

August 2012

There is a crack in everything. That's how the light gets in. - Leonard Cohen

To Pete

Acknowledgments

I would like to thank everyone who helped me get here: Prof. Michael Marder, Prof. Allan MacDonald, my parents, Edgar and Cynthia, my grandparents, Meri, Edgard, and Heloisa, and my family, Peter Bryant and his family, the members of the CNLD and Olga Vera, the members of the MacDonald's group and Becky Drake, my committee members, Prof. Arno Bohm, Prof. Alex Demkov, Prof. Rod Ruoff, and Prof. Maxim Tsoi, the UT-Austin physics department faculty and staff, Prof. Caio Lewenkopf, Prof. Raul Vallejos, Prof. Ildeu de Castro Moreira, Prof. Kirill Bolotin, Hiram Conley, Prof. Rui Huang, Insun Jo, the RLM recycling volunteers, and all my friends.

I thank Fulbright and CAPES for scholarship funding and the National Science Foundation for funding through DMR 0701373.

Ripples and Cracks in Graphene

Publication No. _____

Maria João Brito Moura, Ph.D.
The University of Texas at Austin, 2012

Supervisors: Michael Marder
Allan MacDonald

Graphene is a single layer two-dimensional honeycomb lattice of carbon atoms. It is one of the toughest, lightest, and most conductive materials known. Graphene was first isolated using adhesive tape in 2004, and awarded the Physics Nobel Prize in 2010.

Here we focus on the mechanical properties of graphene. First we present an analytical study, together with numerical simulations, of ripples in graphene. We show that ripples observed in free-standing graphene sheets can be a consequence of adsorbed OH molecules sitting on random sites. The adsorbates cause the bonds between carbon atoms to lengthen slightly.

In the second part of this work we study the fracture mechanics of graphene. Experiments on free-standing graphene can expose the graphene sheets to out-of-plane forces. Here we show that out-of-plane forces can cause free-standing graphene to fracture. This fracture mode is known as the tearing

mode and is common in materials such as paper. We present a numerical study of the propagation of cracks in clamped, free-standing graphene as a function of the out-of-plane force. We also obtain an analytical expression for the minimum force required to tear a two dimensional sheet, which is our model of graphene, in terms of the initial crack length.

Table of Contents

Acknowledgments **v**

Abstract **vi**

List of Tables **xi**

List of Figures **xii**

Chapter 1. Introduction **1**
1.1 A brief history of graphene 1
1.2 Motivation for this work 5

Chapter 2. Ripples in graphene **8**
2.1 Motivation 8
2.2 Free-standing graphene: first experiment and theoretical problems 9
2.3 Thermal fluctuations (membrane theory) 14
2.3.1 Previous studies 16
2.3.2 Frequency of thermally excited ripples 17
2.4 The Mermin-Wagner theorem 18
2.5 Surface impurities and edge effects: simulations and results . . 20

Chapter 3. Cracks in graphene **29**
3.1 Motivation 29
3.2 Analytical approach to tearing a two dimensional sheet 30
3.3 Sheet with an edge crack 34
3.3.1 Analytical study of a sheet with an edge crack 34
3.3.1.1 Small bending approximation 37
3.3.2 Numerical study of a sheet with an edge crack 39
3.4 Sheet with a crack in the middle 48

3.4.1 Analytical study of a sheet with a crack in the middle . 48
3.4.2 Numerical study of a sheet with a crack in the middle . 49
3.4.2.1 Crack in the middle of the sheet generated by defects 49
3.4.2.2 Crack in the middle of the sheet generated by a wide opening 52
3.5 Improved theory - crease energy 56
3.5.1 Energy for a bending strip (no small bending approximation) 56
3.5.2 One-dimensional crease energy 59
3.5.3 Two-dimensional crease energy 61
3.5.4 Griffith Point 64
3.5.5 Numerical study of improved theory 66
3.5.5.1 Numerical study of a sheet with a crack in the middle 67
3.5.5.2 Numerical study of sheet with an edge crack . . 71
3.6 Experiments 74

Chapter 4. Results and conclusions 81
4.1 Ripples in graphene 81
4.2 Cracks in graphene 86
4.2.1 Numerical studies 86
4.2.2 Analytical studies 88
4.2.3 Conclusions 90

Appendices 93

Appendix A. About the code 94

Appendix B. Modified Embedded Atom Method (MEAM) 96

Appendix C. Numerical calculation of graphene's surface energy density Γ 99

Appendix D. Movies of crack propagation 101

Appendix E. Table of numerical results **103**

Bibliography **104**

Index **114**

Vita **115**

List of Tables

E.1 Table of minimum downward force for an initial crack to run on a 100Å by 100Å graphene sheet. 103

List of Figures

1.1 Image from [23]: Graphene wrapped into a buckyball, rolled into a nanotube, stacked to become graphite. 2

1.2 Image from [39]: SEM image of stacked thin platelets of HOPG on a Si(001) substrate. 3

1.3 Image from [53]: AFM image of single-layer graphene. Colors: dark brown, SiO_2 surface; brown-red (central area), 0.8nm height; yellow-brown (bottom left),1.2nm; orange (top left), 2.5nm. Notice the folded part of the film near the bottom, which exhibits a differential height of 0.4nm. 4

2.1 Image from [45]: TEM image of free-standing graphene sheet, scale bar of 500nm. 10

2.2 Image from [45]: *a* and *b* TEM images of folded edges of single and bilayer graphene sheet. Scale bar 2nm. *c*, *d* and *e* Nanobeam electron diffraction patterns from the flat areas as a function of incidence angle. Three different tilt angles for the graphene membrane of Fig. 1.2. *f* and *g* Graph of intensity versus tilt angle for single and bilayer graphene, respectively. The dashed lines are numerical simulations. 12

2.3 Image from [45]: *a* and *b* Flat and corrugated graphene sheet in real space, respectively. *b* is an image of the quantitatively roughness found experimentally. *c* 3D Fourier transform of a flat graphene sheet. *d* and *e* Corrugated sheet, the rods of the reciprocal lattice turn into cone-shaped volumes and the diffraction spots become blurred at large angles. *f* Evolution of diffraction peaks with tilt angle for single layer graphene. Resembles the schematic view of *e*. The blue curves are the intensities for two cases, 0^o and 34^o. *g* Full Width Half Maximum versus tilt angle, for monolayer, bilayer and thin graphite. Dashed lines are the linear fits, that yields the average roughness. The flat region between 0^o to 5^o is due to the intrinsic peak width for the microscope. 15

2.4 Image from [19]: Radial distribution function for the N=8,640 atom sample at T=300 K and T=3,500 K as a function of interatomic distance. The arrows indicate the length of double (r = 1.31Å), conjugated (r = 1.42Å) and single (r = 1.54Å) bonds. 25

2.5 Ripples in graphene produced by edge effects alone in graphene sheet simulated by MEAM, 100Å × 100Å. 26
2.6 Slice through system shown in Figure 2.5 showing that the ripples decay with a characteristic distance of about 3Å away from the edge of the graphene sheet. 26
2.7 Ripples in graphene produced by 20% coverage of OH, 200Å × 200Å system. 27
2.8 Wavelength and amplitude of buckles versus OH concentration in 200Å × 200Å sheets. Amplitudes of the rippled peaks are around six times larger than the rms amplitude. Wavelength and rms amplitude were computed after excluding 20Å of material at the edge of the sample. Wavelength was computed by decomposing the sheet into a series of line scans, taking the one-dimensional Fourier transform of them in turn, finding the average wave vector $\bar{k}$ for each line weighted by the amplitude of the Fourier transform, computing $\lambda = 2\pi/\bar{k}$ and finally averaging λ over all the line scans. Error bars represent standard errors after averaging over three independent trials per concentration. 28

3.1 Image from [67]: SEM imagine of free-standing graphene membrane with partial tears in the surface. 30
3.2 Fig. 3.2a image from [62]: Mode I fracture in a monolayer graphene. Atoms at the outer boundary (red) are fixed, while the remaining atoms (green) are free. Fig. 3.2b image from [27]: Tearing of graphene nanoribbons (along the armchair and the zigzag directions). 31
3.3 Top image: Clamped, free-standing two dimensional sheet with an initial crack of length l at the right hand side. Bottom image: Because of an external downward force the crack runs, a length dl, and the sheet bends diagonally. 33
3.4 One dimensional strip of length L, fixed at one end, and bending due to an external downward force. 35
3.5 Clamped, free-standing two dimensional sheet with an initial crack of length l. The dashed square is the part of the sheet that is initially free-to bend, as it is not attached to the support. The sheet bends because of the applied downward force. . . . 36
3.6 Zooming on Fig. 3.5: two dimensional sheet of sides of length l and diagonal length L. The sheet bends because of the applied downward force. 36

3.7 Initial edge crack of $l \approx 10$Å in a 100Å by 100Å clamped, free-standing graphene sheet. 40
3.8 Constant downward force is applied on the sheet of Fig. 3.7. Initially the sheet wrinkles and bends. 40
3.9 Downward constant force is applied on the sheet of Fig. 3.7. After the sheet wrinkles and bends the crack propagates. . . . 41
3.10 Non-straight crack propagation in a 100Å by 100Å graphene sheet with an initial crack of $l \approx 25$Å. Note that the initial zigzag crack propagates as armchair. 42
3.11 Non-straight crack propagation in a 100Å by 100Å graphene sheet with an initial crack of $l \approx 30$Å. Note that the initial zigzag crack propagates as armchair and then turns zigzag again. 43
3.12 Graph of potential energy (in Joules) vs time step for an initial edge crack of $l \approx 35$Å. The first large drop in potential energy happens while the sheet ripples and bends. Then potential energy slowly decreases as the ripples disappear and the sheet reaches its fully bent state. Another fast drop in potential energy occurs when the crack starts running. 45
3.13 Log-log graph of force (in Newtons per atom) vs initial crack length (in meters) for an edge crack. The line is the theoretical expression, Eq. (3.13), and the plus symbols are the numerical results. 47
3.14 Initial crack of ≈ 10Å in length and ≈ 2Å in width in a 100Å by 100Å clamped, free-standing graphene sheet. 49
3.15 A uniform constant downward force is applied on the sheet of Fig. 3.14. First the sheet wrinkles and bends and then the crack propagates. 50
3.16 Log-log graph of force (in Newtons per atom) vs initial crack length (in meters) for a sheet that exhibits defects. The line is the theoretical expression Eq. (3.21), and the stars are the numerical results. 51
3.17 Initial crack of $l \approx 25$Å generated by an opening of $\approx 20^\circ$ in a 100Å by 100Å clamped, free-standing graphene sheet. 52
3.18 A uniform constant downward force is applied on the sheet of Fig. 3.17 and the crack propagates. 53
3.19 Log-log graph of force (in Newtons per atom) vs initial crack length (in meters) for a wide-open middle crack. The line is the theoretical expression, Eq. (3.21), and the dots are the numerical results. 54

3.20 Graph of force (in Newtons per atom) vs initial crack length (in meters) . The line is the theoretical expression, Eq. (3.21), the green dots are the numerical results for a wide-open middle crack and the red stars are the numerical results for a sheet that exhibits defects. 55

3.21 Clamped, free-standing graphene sheets with an initial crack (at the edge and in the middle) under a downward constant force. In both cases the sheet exhibits a crease before the crack runs. The crease goes from the crack tip basically all the way to the fixed end. 57

3.22 Suspended sheet with an initial crack of length l. The triangle formed by the crease is the part of the sheet that is initially free to bend, as it is not attached to the support. 61

3.23 Zooming on Fig.3.22: right triangle formed by the crease, $n = n_1 + n_2$, the crack length, l, and the width of the sheet (minus the fixed length), m. 62

3.24 Plot of force (in Newtons per atom) versus initial crack length (in meters), Eq. (3.54). The half width of the sheet, $\tilde{m}$, in Fig. 3.24b is 10 times larger than the one in Fig. 3.24a. 66

3.25 Graph of force (in Newtons per atom) vs initial crack length (in meters) for a wide-open middle crack. The line is the theoretical expression, Eq. (3.54), the dashed line is the approximation $l << m$, Eq. (3.56), and the numerical results are the the dots with the error bars. 68

3.26 Graph of force (in Newtons per atom) vs initial crack length (in meters) for a wide-open middle crack. The line is the theoretical expression, Eq. (3.54), the green dots are the numerical results for a sheet of 100Å $\times$ 100Å, and the orange triangles are the numerical results for a sheet of 200Å $\times$ 100Å. 69

3.27 Log-log graph of force (in Newtons per atom) vs initial crack length (in meters) for a wide-open middle crack. The line is the theoretical expression, Eq. (3.54), the dots are the numerical results for a sheet of 100Å $\times$ 100Å, and the triangles are the numerical results for a sheet of 200Å $\times$ 100Å. 70

3.28 Log-log graph of force (in Newtons per atom) vs initial crack length (in meters) for an edge crack. The line is the theoretical expression, Eq. 3.52, and the plus symbols are the numerical results. 71

3.29 Clamped, free-standing graphene sheets with an initial edge crack under a downward constant force. The sheets exhibits a crease before the crack runs. The crease starts at the crack tip and ends before the fixed end. 72

3.30 Log-log graph of force (in Newtons per atom) vs initial crack length (in meters) for an edge crack. The dashed line is the best fit for theoretical expression, Eq. (3.52), assuming m to be a fitting parameter, and the plus symbols are the numerical results. The width of the sheet minus the fixed ends is 90Å and the best fit value for m is 64Å. 73

3.31 Image courtesy of Hiram Conley, Bolotin Research Group: Fracture in CVD graphene. Note the crease going from the crack on the left side all the way to the fixed edge on the right. . . . 77

3.32 Image courtesy of Hiram Conley, Bolotin Research Group: Fracture in CVD graphene. 78

3.33 Image courtesy of Hiram Conley, Bolotin Research Group: Top view of fracture in CVD graphene. 79

3.34 Graph of force (in Newtons per atom) vs initial crack length (in meters). The line is the theoretical expression for a crack in the middle of the sheet, Eq. (3.54), with $\tilde{m} = 1\mu$m. The dashed line is for a crack at the edge, Eq. (3.56), with $m = 2\mu$m. . . . 80

4.1 Fig. 4.1a Ripples in graphene produced by edge effects alone in graphene sheet of 100Å × 100Å. Fig. 4.1b Ripples in graphene produced by 20% coverage of OH, 200Å × 200Å system. . . . 83

4.2 Wavelength and amplitude of buckles versus OH concentration in 200Å × 200Å sheets. Amplitudes of the rippled peaks are around six times larger than the rms amplitude. Wavelength and rms amplitude were computed after excluding 20Å of material at the edge of the sample. Wavelength was computed by decomposing the sheet into a series of line scans, taking the one-dimensional Fourier transform of them in turn, finding the average wave vector $\bar{k}$ for each line weighted by the amplitude of the Fourier transform, computing $\lambda = 2\pi/\bar{k}$ and finally averaging λ over all the line scans. Error bars represent standard errors after averaging over three independent trials per concentration. 84

4.3 Constant downward force is applied on a 100Å by 100Å clamped, free-standing graphene sheet with an initial crack of $l \approx 15$Å. Notice that the sheet wrinkles and bends before the crack runs. 87

4.4 Clamped, free-standing graphene sheets with an initial edge crack under a constant downward force. Fig 4.4a: The sheets exhibits a crease just before the crack runs. Fig. 4.4b: Non-straight crack propagation - the initial zigzag crack propagates as armchair and then turns zigzag again. 88

4.5 Suspended sheet with an initial crack of length l. The triangle formed by the crease is the part of the sheet that is initially free to bend, because it is not attached to the support. 90

4.6 Graph of force (in Newtons per atom) vs initial crack length (in meters) for a wide-open middle crack. The line is the theoretical expression, Eq. (3.54), the green dots are the numerical results for a sheet of 100Å $\times$ 100Å, and the orange triangles are the numerical results for a sheet of 200Å $\times$ 100Å. Note that long cracks on the 100Å $\times$ 100Å sheet are influenced by edge effects. 92

C.1 Graph of energy per length (in Joules per meter) vs downward distance (in meters). 100

Chapter 1

Introduction

1.1 A brief history of graphene

Graphene is a single layer 2D honeycomb lattice of carbon atoms. Theoretically, from graphene it is possible to obtain all graphitic structures (Fig. 1.1). A stack of graphene sheets forms 3D graphite. A rolled graphene sheet forms a nanotube. And a wrapped graphene sheet becomes a bucky-ball. Graphene is one of the toughest, lightest, and most conductive materials known.

The first experiments to observe monolayer graphite where done in the 1970s by Jack Blakely's group at Cornell University [18]. In the 1990s a search for a more reliable and controllable technique to obtain graphene sheets started, motivated by the discovery of carbon nanotubes. "It might be possible, by the controlled fabrication of graphene sheets, to form nanotubes or other novel motifs of use for nanotechnology" said the experimental group of Rodney Ruoff's when, in 1999, they rubbed tailored micropillars of highly oriented pyrolytic graphite (HOPG) against a silicon substrate and obtained neat looking stacks of thin layers of graphene spread out like a deck of cards [39, 40] (Fig. 1.2). Similarly, in 2004, Philip Kim's group used a block of

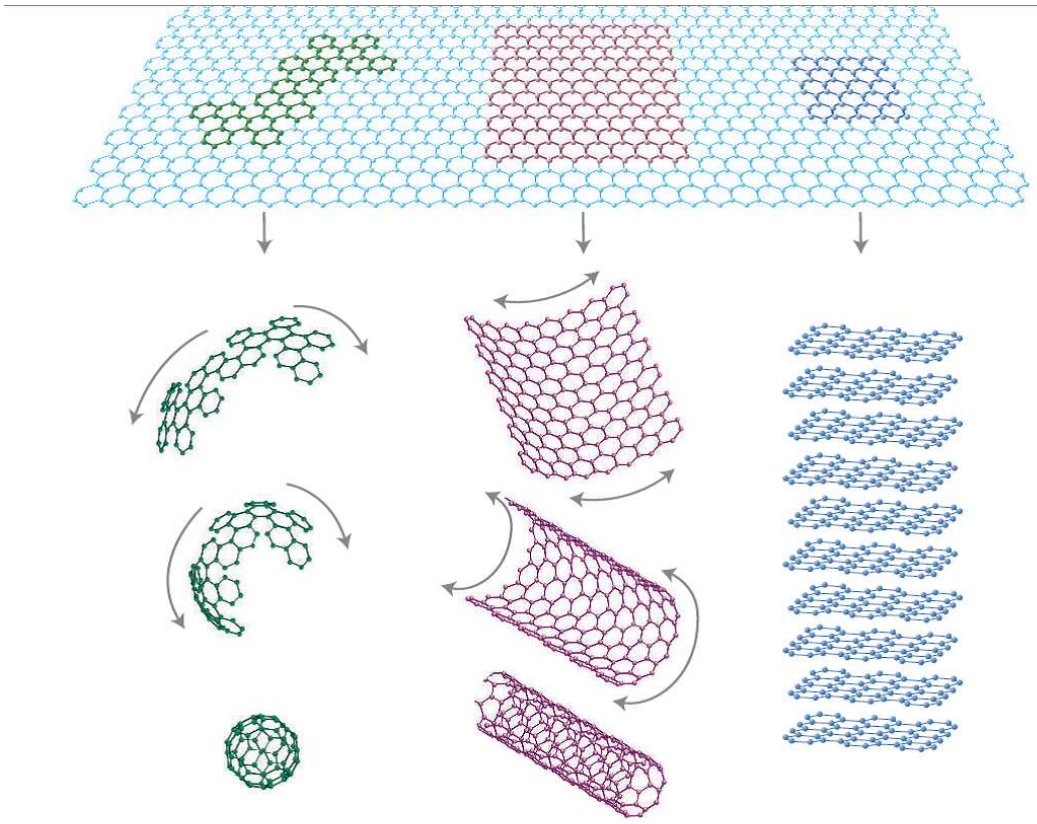

Figure 1.1: Image from [23]: Graphene wrapped into a buckyball, rolled into a nanotube, stacked to become graphite.

graphite mounted on a cantilever as the tip of an atomic force microscope (AFM) and was able to shear off layers of HOPG, with thicknesses ranging from 10 to 100nm, onto a silicon substrate [68].

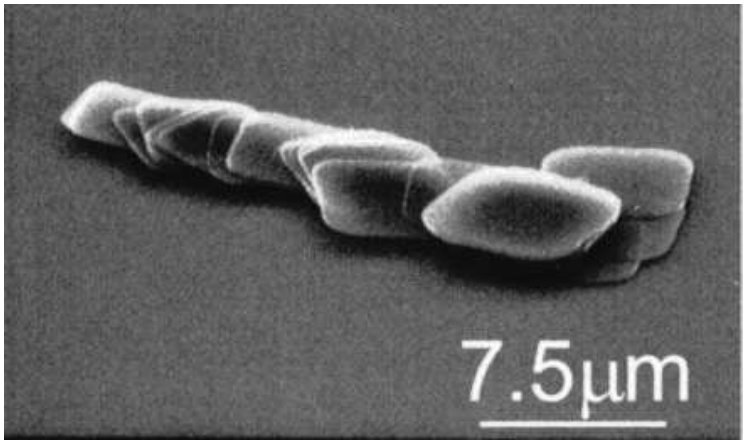

Figure 1.2: Image from [39]: SEM image of stacked thin platelets of HOPG on a Si(001) substrate.

In 2004, Andre Geim's group at the University of Manchester presented a new consistent method of producing and identifying graphene samples [53]. In the micromechanical cleavage method, also known as the scotch tape method, a graphite sample is peeled out with scotch tape and then deposited on a SiO_2 substrate (Fig. 1.3). This experimental technique generates multi and single layer graphene. Andre Geim and Konstantin Novoselov were awarded the 2010 Physics Nobel Prize "for groundbreaking experiments regarding the two-dimensional material graphene".

Currently there are many other methods to obtain few-layer graphene, such as epitaxial growth, by chemical vapor deposition of hydrocarbons on

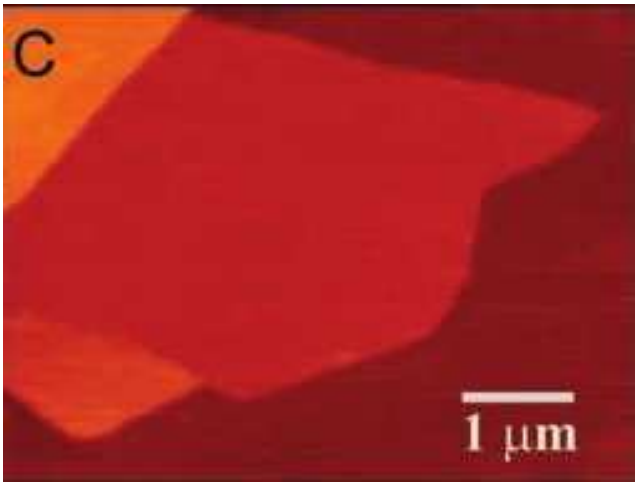

Figure 1.3: Image from [53]: AFM image of single-layer graphene. Colors: dark brown, SiO_2 surface; brown-red (central area), 0.8nm height; yellow-brown (bottom left),1.2nm; orange (top left), 2.5nm. Notice the folded part of the film near the bottom, which exhibits a differential height of 0.4nm.

metal substrates [31, 49] and by thermal decomposition of SiC [11, 20, 55, 65]. Also "chemical exfoliation" [16] of graphite oxide is a variation that results in graphene oxide [59, 60].

Strictly speaking graphene is a one atom thick sheet, but sometimes few layer structures are also referred to as graphene (or as "few-layer graphene"). From the experimental point of view the thickness of a graphene sheet is hard to determine, and it is still a point of controversy in the literature [54].

Like nanotubes, graphene presents many attractive properties to basic science and to industry. It is light, flexible, practically transparent, and thermally stable (in a non-oxidizing environment). It presents a high electrical conductivity (the Fermi velocity of electrons in graphene is 10^6 m/s) and dis-

plays an anomalous integer Quantum Hall Effect even at room temperature. And while nanotubes with different types of "twist" (called: armchair, zigzag and chiral) can be metals or semiconductors, graphene presents the unique and very interesting property of being a zero-gap semiconductor [53, 54].

However there are still practical difficulties to be overcome. The current methods of fabrication are not able to produce massive quantities of graphene with consistent sizes and electronic properties, and so, for graphene to be considered for industrial applications, better methods need to be developed. A better understanding of graphene's electronic and mechanical properties is fundamental to the production of graphene in large scale.

1.2 Motivation for this work

The study of graphene is an attractive field not only because of graphene's extraordinary properties, but also because, as it is a new material, fundamental questions need to be answered and basic properties need to be obtained. The problems addressed in this work are a good example of that.

In 2007 Meyer *et al.* reported that they were able to fabricate free-standing graphene sheets, and that the sheets exhibit ripples [45]. Many thought that producing graphene sheets without a substrate was not possible, because, according to the Mermin-Wagner theorem [44], two-dimensional crystals with long-range order cannot exist at nonzero temperatures. That raised the questions: Is it the ripples that keeps free-standing graphene stable? And what is the effect of these ripples on graphene's electronic and

mechanical properties?

The work of Meyer *et al.* raised other fundamental questions, such as how does a finite size graphene sheet (1 atom thick carbon honeycomb lattice) behave in free space? Theoretically, we are used to thinking of an infinite number of sheets (graphite) or of periodic boundary conditions, but in experiments edges may play an important roll in the crumpling, as well as in other properties of graphene sheets. Also, how do thermal fluctuations affect these one atom thick sheets? And how do we expect a graphene sheet to behave in an experimental set up (clamped both sides, on top of a substrate, on a grid, etc.)?

In the next chapter we address most of these topics. We show that the Mermin-Wagner theorem is not relevant to free-standing graphene, that the ripples observed in the experiments are not due to thermal fluctuations, and that edge effects and impurities cause finite-sized graphene sheets to exhibit ripples.

In the second part of this work we focus on the problem of fracture of free-standing graphene. In some experimental setups free-standing graphene samples show cracks and holes, and sometimes the samples even break [2, 3, 5, 30, 67]. An example of that is the back-gate voltage experimental setup, in which the sheets are exposed to out-of-plane forces. Fracture occurs because of flaws in the material. The questions in this case are: what is the size and geometry of cracks that appear in graphene samples? What is the minimum out-of-plane force that would make such sheets break? And how does that

force compare to the forces the sheets are exposed to in experiments?

Here we show that out-of-plane forces can cause free standing graphene to fracture. This fracture mode is known as the tearing mode and is common in materials such as paper. We also obtain an expression for minimum downward force required for a crack of a certain length to run on a two-dimensional sheet, such as graphene.

In general the fracture of free-standing graphene sheets is an undesirable occurrence. Therefore most experiments do not report or take measurements of such events. However, controlled tearing of graphene sheets might have interesting applications. The edge orientation of a graphene nanoribbon determines its electronic properties, therefore it will be most useful to be able to predict the edge orientation of produced samples.

Chapter 2

Ripples in graphene

2.1 Motivation

Experiments on free-standing graphene sheets [45] observe that the sheets display ripples. The ripples are 2 to 20Å high and 20 to 200Å wide. The sheets in which they appear are one atom thick, and extend for around 5000Å through vacuum between metal struts that support them.

The ripples were explained to be a result of thermal fluctuations [8, 19]. It was also suggested that buckling out-of-plane provides stability to the 2D graphene sheet [15, 19, 23, 45], as, according to the Mermin-Wagner theorem [43], two dimensional crystals are not stable.

In this chapter we show that the ripples observed in these experiments are not due to thermal fluctuations. We also explain that the Mermin-Wagner theorem is not relevant to free-standing graphene sheets.

We propose a different mechanism to the rippling of graphene sheets: adsorption of impurities at random sites throughout the crystal. It is common for graphene samples to be exposed to the environment, therefore adsorbing impurities such as water, OH, H, etc. [17, 24, 47]. Here we present numerical simulations of graphene sheets with surface impurities.

The work presented in the chapter was done in collaboration with Rebecca Thompson-Flagg and it was published in the paper "Rippling of graphene" [64].

2.2 Free-standing graphene: first experiment and theoretical problems

The first report of free-standing graphene sheets came out on March of 2007 in a paper entitled "The structure of suspended graphene sheets" [45]. In this work, TEM (transmission electron microscope) images of graphene sheets freely suspended on top of a microfabricated metal scaffold in vacuum or air are presented, see Fig. 2.1, and diffraction patterns obtained from these sheets are shown, Fig. 2.2. This paper contains three main ideas: it is possible to fabricate free-standing graphene; one can distinguish between single and multilayer structures by looking at intensity versus tilt angle of the diffraction peaks of the sheets; and graphene sheets obtained by this method exhibit ripples. In this section we will discuss these topics and the consequences of this experiment to the understanding of graphene properties.

The procedure for fabricating free-standing graphene is the following: first the graphene sheets are obtained by the standard method of micromechanical cleavage (see Sec. 1.1 and [53]), and single layer sheets are identified by optical microscopy. The second step is to deposit a metal grid (made of 100nm of Au and 3nm of Cr) on top of the sample, using electron-beam lithography. After a number of etching steps the substrate is wiped out and the structures

Figure 2.1: Image from [45]: TEM image of free-standing graphene sheet, scale bar of 500nm.

left are graphene crystallites on top of the microfabricated scaffold.

By examining the TEM image of the suspended graphene sheet, Fig. 2.1, the authors observed that it shows folds and scrolls, especially at the edges.

One way to identify single and multilayer graphene presented by the authors is based on the intensity of the diffraction peaks of a sample. The electron diffraction patterns of a single layer graphene sheet are shown on Fig. 2.2 *c*, *d*, and *e*. To find the intensity values, each of the Bragg reflections was fitted by a Gaussian distribution for every angle, which yielded the peak intensities, as well as positions, heights, and widths. Graphs of intensity versus tilt angle of the diffraction peaks are shown in Fig. 2.2 *f* and *g* for single and bilayer samples, respectively. Constant intensity with weak monotonic variation is a clear signature for a single layer (see Fig. 2.2 *f*).

One interesting effect that is seen in all diffraction images is the broadening of the peaks, which, from the theory of diffraction of 3D crystals, is unexpected. This broadening shows three main characteristics: it increases the farther away the peak is from the axis, without change in intensity; it is isotropic; and it is weaker in bilayer and disappears in multilayer graphene systems. The authors comment that thermal vibrations can only reduce the intensity of diffraction peaks, but not broaden them, and so thermal vibrations cannot yield this effect.

The explanation for the broadening is that the graphene sheets observed are in fact not flat within the submicrometre area of the electron beam. Fig. 2.3

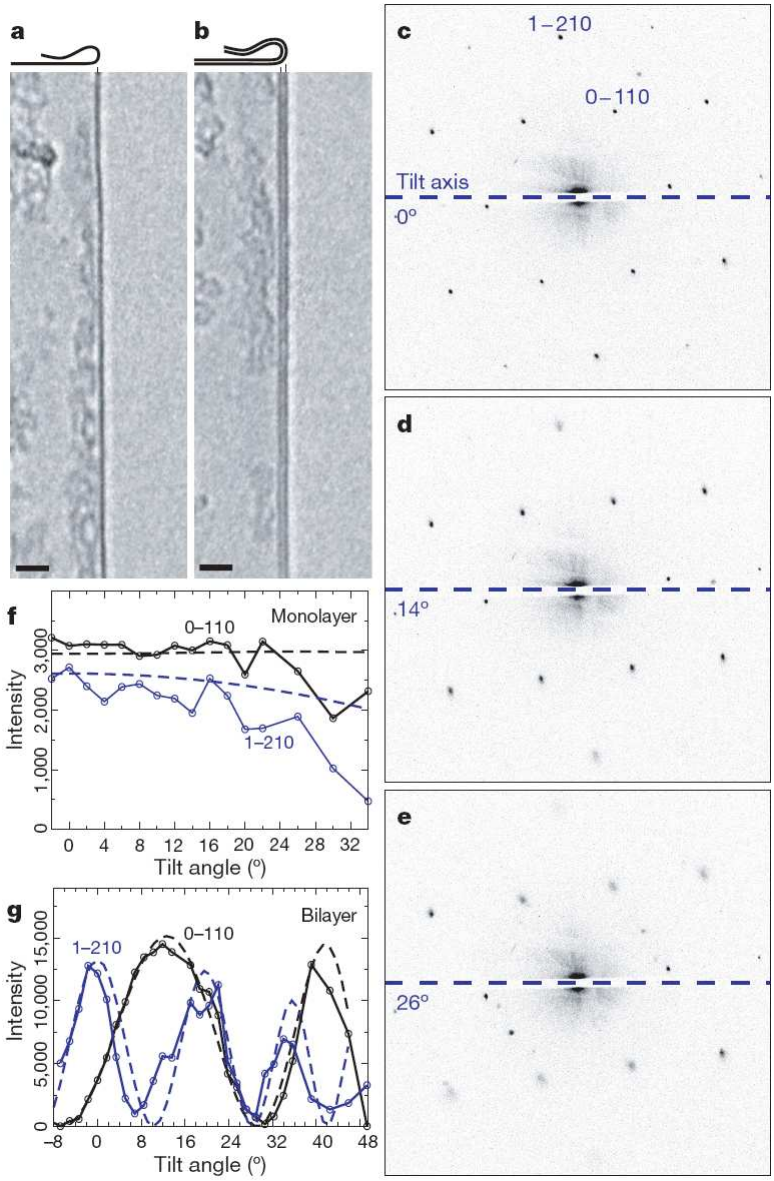

Figure 2.2: Image from [45]: *a* and *b* TEM images of folded edges of single and bilayer graphene sheet. Scale bar 2nm. *c*, *d* and *e* Nanobeam electron diffraction patterns from the flat areas as a function of incidence angle. Three different tilt angles for the graphene membrane of Fig. 1.2. *f* and *g* Graph of intensity versus tilt angle for single and bilayer graphene, respectively. The dashed lines are numerical simulations.

$c - e$ shows a scheme of how these ripples appear. The 3D reciprocal lattice of a flat graphene sheet is a hexagon (as known from the 2D structure) with rods at each end, Fig. 2.3 c. When the sheet becomes corrugated, Fig. 2.3 d, a superposition of the diffracting beams from microscopic flat areas turns the rods into cone-shaped volumes, so that diffraction spots become blurred at large angles (dotted lines in Fig. 2.3 e), and the effect is more pronounced farther away from the tilt axis (note the peaks farther away from the axis in Fig. 2.2). The authors explain that if the corrugations were not static, the changes would lead to blurring of the atomic-resolution images, which is not seen.

The crumpling size is inferred from two parameters [4]. First, the ratio of height to width of the ripples is directly given by the cone angle (Fig. 2.3 $d - f$): The cone angle of 10° gives the variation in the surface normal, corresponding to a ratio height to width of ~ 0.1. The authors claim that this is a precise measurement.

The width (lateral size) of the ripples is estimated from the transverse coherence of the electron beam ($\sim$ 20 to 200Å) and the illuminated area for one diffraction pattern (2500Å). Essentially, the width must be much smaller than the 2500Å illuminated area (by around an order of magnitude, giving an upper limit of $\sim$ 250Å), but it cannot be smaller than the coherence length. This leaves quite a range, between 20 to 250Å for the lateral size of the ripples. Then the height, as described above, is 10% of the width, therefore between 2 and 20Å. Note that the C-C bond length in graphene is 1.42Å, hence the

crumpling wavelength is much bigger than the C-C bond distance.

The authors give two arguments for the crumpling of the graphene sheets. First, they propose that according to the Mermin-Wagner Theorem [32, 43] "perfect two-dimensional crystals cannot exist in the free state", "thermal fluctuations should destroy long-range order, resulting in melting of a 2D lattice at any finite temperature," and "the observed corrugations in the third dimension may provide subtle reasons for the stability of two-dimensional crystals". Second, by making an analogy between graphene sheets and membranes, the authors comment that considering "beyond the harmonic approximation has led to the conclusion that the interaction between bending and stretching long-wavelength phonons could in principle stabilize atomically thin membranes through their deformation in the third dimension" [50, 51].

Further discussion of the comparison of graphene sheets and membranes will be presented on Sec. 2.3. And the fact that the Mermin-Wagner theorem is not relevant to free-standing graphene sheets will be presented in Sec. 2.4

2.3 Thermal fluctuations (membrane theory)

Since the first report on free-standing graphene there have been multiple publications about the origin and effects of the crumpling of such sheets [8, 19, 26, 29, 58, 61]. In this section we discuss the possibility that the ripples are due to thermal fluctuations.

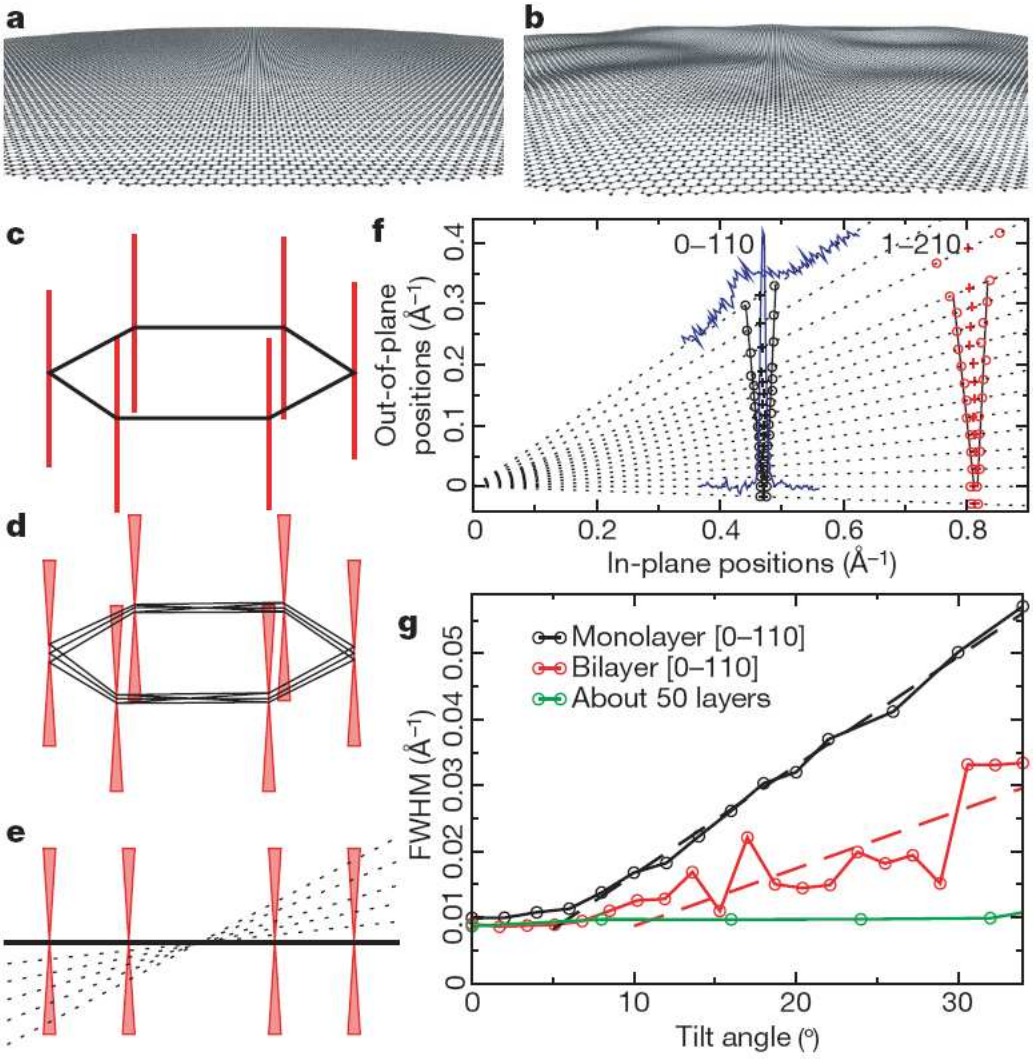

Figure 2.3: Image from [45]: *a* and *b* Flat and corrugated graphene sheet in real space, respectively. *b* is an image of the quantitatively roughness found experimentally. *c* 3D Fourier transform of a flat graphene sheet. *d* and *e* Corrugated sheet, the rods of the reciprocal lattice turn into cone-shaped volumes and the diffraction spots become blurred at large angles. *f* Evolution of diffraction peaks with tilt angle for single layer graphene. Resembles the schematic view of *e*. The blue curves are the intensities for two cases, 0^o and 34^o. *g* Full Width Half Maximum versus tilt angle, for monolayer, bilayer and thin graphite. Dashed lines are the linear fits, that yields the average roughness. The flat region between 0^o to 5^o is due to the intrinsic peak width for the microscope.

2.3.1 Previous studies

In the paper "Intrinsic ripples in graphene" [19] Fasolino *et al.* discuss the applicability of phenomenological theories for flexible membranes (continuum limit, no microscopic feature) to graphene for a wide range of temperatures (T) and sample sizes. The computational approach used to treat fluctuations was atomistic Monte Carlo simulations, based on a many-body interatomic potential for carbon (LCBOPII). The simulations consider a square lattice, with periodic boundary conditions, and a flat initial configuration. The temperatures range from 300 to 3500 K. Ripples spontaneously appear owing to thermal fluctuations. No defects are observed. The crumpling size for $T = 300$K is ~ 0.7Å high and ~ 80Å wide. Note that the crumpling height is 3 to 30 times smaller than the observed in experiments [45]. The authors suggest that the ripples are due to the multiplicity of chemical bonding in carbon, Fig. 2.4. We observe similar effects in our simulations. Though in their case it is caused by thermal fluctuations, while in our case it is due to impurities attached to the graphene sheet. We will discuss this further in Sec. 2.5.

Fasolino *et al.* compared their simulations with the theory of flexible membranes [50, 51], considering harmonic and anharmonic couplings. They concluded that the harmonic approximation, in which bending and stretching modes are decoupled, is quite accurate. The anharmonic coupling was shown to stabilize the flat phase [34].

Abedpour *et al.* [8] obtained similar rippling patterns studying structures of 500 by 500 carbon atoms. The simulations were performed using

the Tersoff-Brenner empirical potential [14] and considered periodic boundary conditions. The thermal fluctuations were analyzed with the Nose-Hoover thermostat for temperatures between 10 and 300 K.

Abedpour *et al.* also showed that the roughness of the graphene sheets can result in a magnetic field, which can have consequences for the electronic structure of these sheets. Kim *et al.* [29] obtained similar results.

2.3.2 Frequency of thermally excited ripples

The energy of a thin membrane is approximately given by [32]:

$$E = \int d^2r \left[\frac{1}{2}\rho\dot{z}^2 + \frac{k}{2}\left(\nabla^2 z\right)^2\right], \tag{2.1}$$

where z is the out-of-plane displacement, ρ is the mass per area, and k is the bending modulus. The first term in the equation above is the kinetic energy and the second one is the bending energy. Here we consider that stretching modes are negligible. Therefore thermally excited ripples of wavenumber ζ should oscillate at a frequency ω given by:

$$\omega^2 = \frac{k}{\rho}\zeta^4. \tag{2.2}$$

The density of graphene is $\rho = 7.60 \times 10^{-7}$ Kg/m^2. At room temperature the bending modulus of graphene is $k \approx 1$eV [19, 52, 64] and the ripples observed have wavelengths of 20 to 200Å. Hence the frequency of these thermally excited ripples is between 10^9 and 10^{11}Hz. Such rapid oscillations cannot be resolved in diffraction experiments, thus they should produce sharp

Bragg peaks. However the experiments [45] observe broad peaks, therefore the ripples observed in free-standing graphene should be static and not caused by thermal fluctuations.

2.4 The Mermin-Wagner theorem

A common argument, based on the Mermin-Wagner theorem [43], is that free-standing graphene sheets ripple because two-dimensional crystals are not stable. This statement is found in many papers [15, 19, 23, 45] and even on Wikipedia, but it is incorrect. Garcia *et al.* [21] also discuss the misuse of the Mermin-Wagner theorem for free-standing graphene.

It is important to understand that the Mermin-Wagner theorem is correct, but it is not relevant for free-standing graphene sheets. The theorem states that long-range crystalline order is not possible in two dimensions, it is destroyed by fluctuations at any nonzero temperature. That does not mean that real 2D systems are liquid at any nonzero temperatures, instead it means that Bragg peaks are broadened. The broadening of diffraction peaks is also observed in systems that exhibit quasi-long-range order, which means they do not have long-range positional order, but they do have orientational order, such as hexatic crystals [42, 48].

There is not enough experimental evidence to support the idea that the graphene sheets used in these experiments exhibit long-range crystalline order. And for finite-sized samples the deviations from long-range order may not be very large.

According to the Mermin-Wagner theorem, for a two-dimensional crystal to remain completely planar it has to undergo rotations at large distances, these cause a breakdown of long-range order. Here we estimate the distance D at which the loss of long-range translational order occurs in graphene samples.

Let us call the vector field that describes the displacement of every point in the solid $\overrightarrow{u}$. The average square displacement of particles from their original location is given by [42]:

$$\langle u^2 \rangle = 2 \int \frac{d^2q}{(2\pi)^2} \frac{k_B T}{G q^2} \tag{2.3}$$

where q is the wave vector, G is the shear modulus of graphene, k_B is the Boltzman constant, and T is the temperature.

We should cutoff the integral at the lattice spacing a, where continuum mechanics breaks down, and at D to find the distance at which the loss of long-range order occurs. Hence:

$$\langle u^2 \rangle \approx \int_{1/D}^{1/a} q dq \frac{k_B T}{G q^2} \tag{2.4}$$

which results in:

$$\langle u^2 \rangle \approx \frac{k_B T}{G} \ln\left(\frac{D}{a}\right) \tag{2.5}$$

Therefore the distance at which the loss of long-range order occurs is given by:

$$D \approx a \exp\left(\frac{G\langle u^2 \rangle}{k_B T}\right). \tag{2.6}$$

The experiments are performed at room temperature. The bulk shear modulus $\mu \approx G/a$ of graphite is 440 GPa [56]. The lattice spacing of graphene

is $a \approx 1$Å. Considering deviations of the order of a lattice spacing, $u \approx a$, we obtain $D > 10^{30}$ m. And even smaller deviations, for example, of about 10% of the size of the lattice spacing, result in $D \approx 2$mm. In any case the scale at which the loss of long-range order occurs is much lager than the graphene samples, so rotations should be irrelevant.

2.5 Surface impurities and edge effects: simulations and results

The fact that the graphene sheet ripples means that there is a change in the equilibrium distance between carbon atoms in some, but not all parts of the sheet. Fasolino *et al.* observed such effect in their numerical study of thermal fluctuations in graphene [19]. However we have shown that the ripples are static, therefore they must be due to a different mechanism.

Our first step was to study a free finite-sized graphene sheet, to understand the effects of under-coordinated edge atoms. To do so we use the Modified Embedded Atom Method (MEAM) potential [9], shown to reproduce well the properties of graphene [35]. MEAM is a semi-empirical interatomic potential, based on density functional theory (it considers the superimposition of atomic density). Our implementation of this potential has been tested extensively in simulations of cracks in silicon [25] and shock waves in tin [33]. The energy minimization is done through damped molecular dynamics. In an effort to better model the experimental conditions, all the simulations in this work are of finite-sized graphene sheets, in contrast to the work of Fasolino *et*

al. [19] and Abedpour *et al.* [8], which relies on periodic boundary conditions. These simulations were done at zero temperature, to focus on effects not due to temperature.

In order to understand the behavior of a free graphene sheet, we keep the edges free (and not saturated) in the simulations. In the experiments the sheets are in vacuum and they free-stand for ≈5000Å between the metal struts that support them.

The system is initially entirely flat, except that atoms are randomly displaced from initial conditions by around 10^{-2}Å. Then the system is allowed to relax toward a minimum energy state through damped molecular dynamics.

A system of 100Å by 100Å is shown in Fig. 2.5. We observe that in fact under-coordinated edge atoms create edge effects. As a results of the lack of neighbors, edge atoms have different chemical bonds than bulk atoms. The change in bond length causes the sheet to come out-of-plane.

Similar results to Fig.2.5 were also obtained independently by Lu along with Huang [7], using Brenner's potential [14], and by Shenoy *et al.*, using an AIREBO potential [58].

The ripples due to edge effects are ≈30Å wide and ≈10Å high. However they occur only at the edge of the system, and the amplitude decays to zero on the scale of 3.2Å (Fig. 2.6). Thus, edge effects alone cannot explain the ripples observed in experiments [45].

In correspondence with A. Geim, we learned that OH molecules could

be expected to be adsorbed on the surface of graphene sheets. It is common for graphene samples to be exposed to the environment, therefore adsorbing impurities such as water, OH, H, etc. [17, 24, 47]. We decided to investigate the effects of surface impurities on free-standing graphene sheets. Details of the molecule are not likely to be critical, and we discuss OH in order to have a specific example. The density of the adsorbates in graphene is not known, so we have treated it as a free parameter, and considered the effects of randomly placing OH molecules on the graphene's surface.

Xu *et al.* [66] have shown that attaching an OH molecule to a carbon surface has the consequence of increasing the length of two adjoining C-C bonds by around 10% (see their Fig. 2, L0D + OH). Simulating the interactions between different atoms is a hard task. Thus, instead of actually adding OH molecules to the surface of the graphene sheet, we simply chose carbon atoms randomly from the lattice, and increased the equilibrium length to two randomly chosen neighbors. For the bonds we wished to stretch, the MEAM parameter Rc was increased from 1.42Å (the bond length of graphene) to 1.48Å. This value was chosen because if used for the entire crystal, it produces an equilibrium lattice parameter close to what Xu *et al.* find for the C-C bonds stretched by OH.

Here, as in the clean-sheet case, we apply a perturbation to the initially flat sheet with free edges and allow it to relax toward a minimum energy configuration.

Our simulations show that impurities on the surface of graphene sheets

cause them to ripple. Fig. 2.7 shows a graphene sheet with a 20% concentration of OH adsorbates. The ripples sizes depend on the impurity concentration.

Fig. 2.8 shows a graph of wavelength and amplitude of buckles versus impurity concentration. The wavelength changes rather little with concentration, while rms amplitude increases. The peak-to-peak amplitudes of the ripples are around six times larger than the rms amplitude. A OH concentration of about 5% has a peak-to-peak amplitude of ≈3Å. At 20% the amplitude reaches ≈6Å. The wavelength for both cases is ≈50Å. The ripples observed in experiments are estimated to be 2 to 20Å high and 20 to 200Å wide [45].

Experimentalists say that 20% concentration of impurities is unlikely to happen on pristine graphene [1, 6]. These would be more likely in graphane (graphene+CH_2) and graphene oxide.

Using a similar method to Tersoff [63] we find, from our simulations, the bending modulus of graphene to be $k = 1.77$eV. The known experimental value is $k_{exp} = 1.2$eV [52]. And Fasolino *et al.* obtained $k = 1.1$eV [19]. As the MEAM potential overstates the bending energy of graphene, it will tend to underestimate the scale of ripples.

Whether this mechanism is in fact responsible for the buckles might be determined by experiments on adsorbate-free surfaces conducted in high vacuum. However, it is worth noting that since Meyer *et al.*'s experiment [45] the understanding of the experimental significance of the presence of adsorbates in graphene has increased. Many graphene samples now pass through

a heat treatment before being used for measurements. Experiments that use processes to reduce impurities on graphene sheets, such as annealing, observe a reduction of the rippling of the sheets [26], in agreement with our simulations.

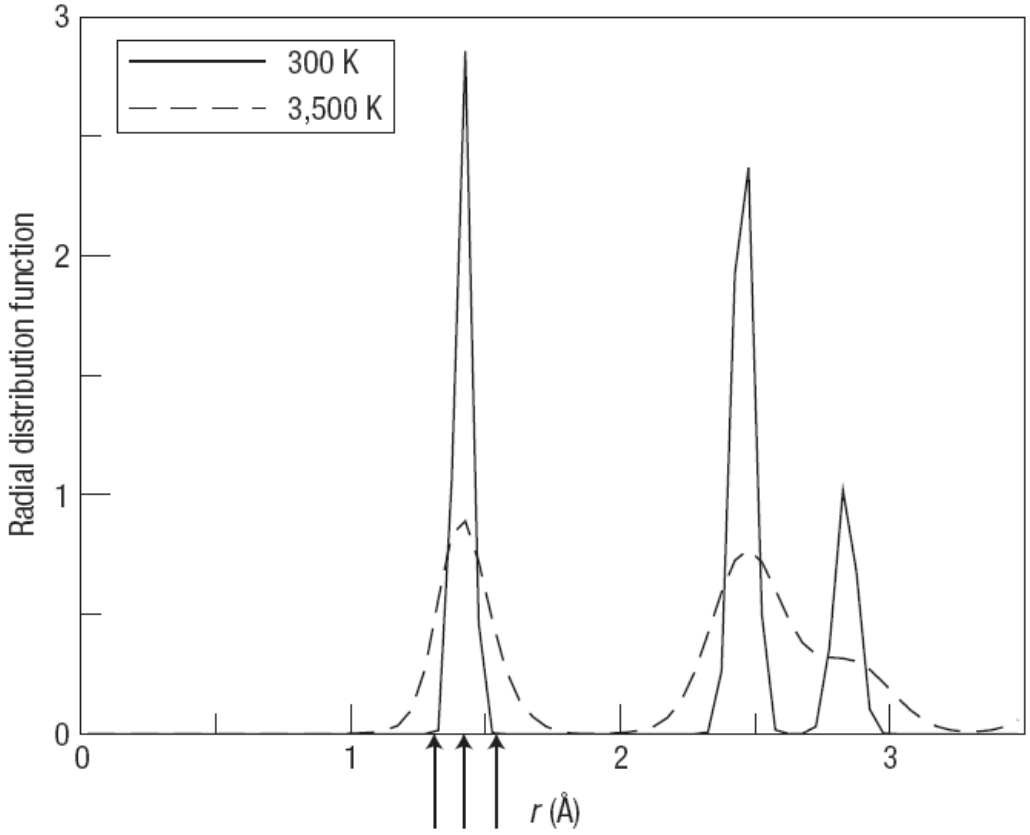

Figure 2.4: Image from [19]: Radial distribution function for the N=8,640 atom sample at T=300 K and T=3,500 K as a function of interatomic distance. The arrows indicate the length of double (r = 1.31Å), conjugated (r = 1.42Å) and single (r = 1.54Å) bonds.

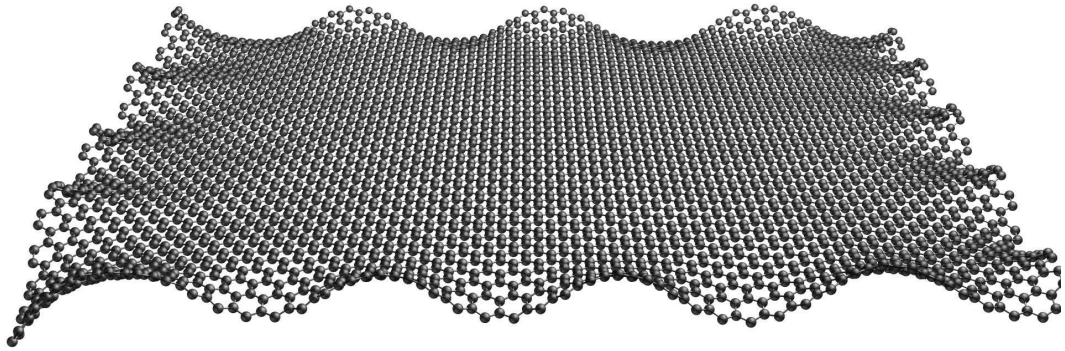

Figure 2.5: Ripples in graphene produced by edge effects alone in graphene sheet simulated by MEAM, 100Å × 100Å.

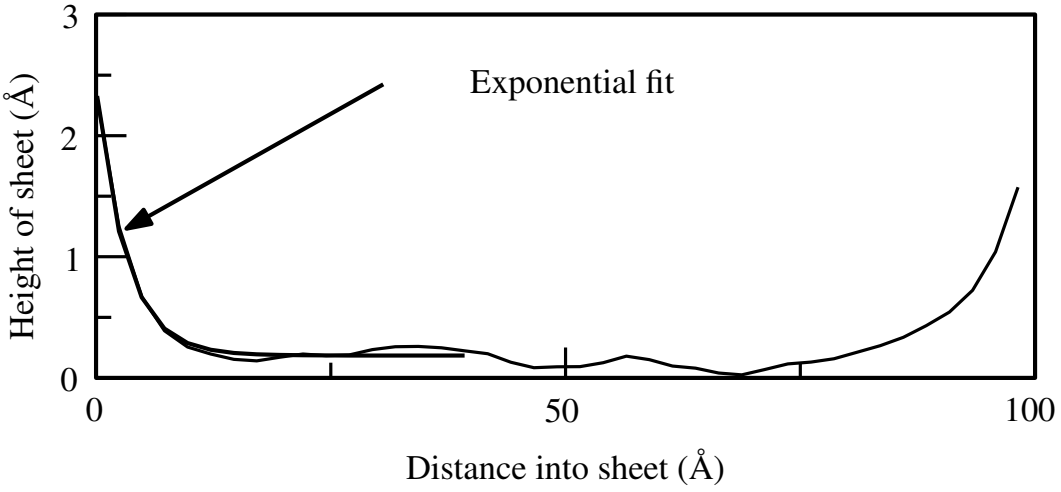

Figure 2.6: Slice through system shown in Figure 2.5 showing that the ripples decay with a characteristic distance of about 3Å away from the edge of the graphene sheet.

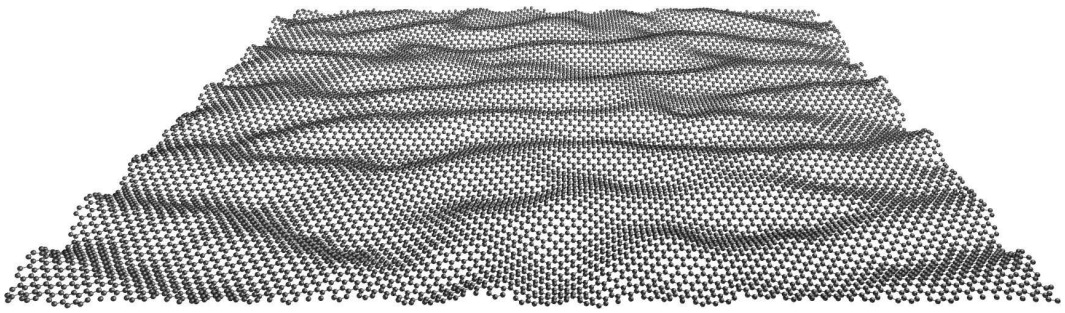

Figure 2.7: Ripples in graphene produced by 20% coverage of OH, 200Å × 200Å system.

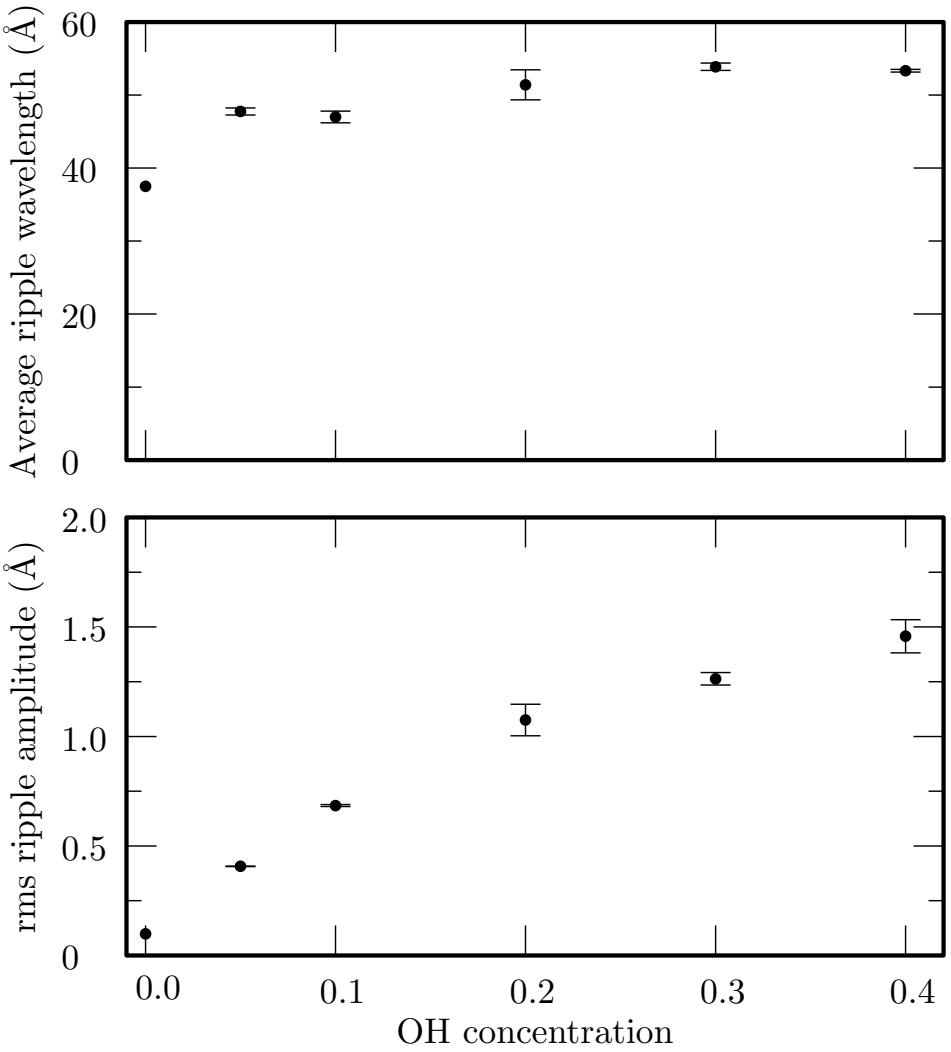

Figure 2.8: Wavelength and amplitude of buckles versus OH concentration in 200Å $\times$ 200Å sheets. Amplitudes of the rippled peaks are around six times larger than the rms amplitude. Wavelength and rms amplitude were computed after excluding 20Å of material at the edge of the sample. Wavelength was computed by decomposing the sheet into a series of line scans, taking the one-dimensional Fourier transform of them in turn, finding the average wave vector $\bar{k}$ for each line weighted by the amplitude of the Fourier transform, computing $\lambda = 2\pi/\bar{k}$ and finally averaging λ over all the line scans. Error bars represent standard errors after averaging over three independent trials per concentration.

Chapter 3

Cracks in graphene

3.1 Motivation

Today many experiments use graphene in the free-standing experimental setup, mostly in an effort to observe better electronic properties in the absence of a substrate [12, 13, 22, 67]. Experiments on free-standing graphene can expose the graphene sheets to out-of-plane forces. In some experimental setups free-standing graphene samples show cracks and holes, and sometimes the samples even break [2, 3, 5, 30, 67], Fig. 3.1. The back-gate voltage experimental setup is an example of a setup where samples have been observed to break. In this setup the free-standing graphene sheet is clamped and exposed to a downward force from an external electric field.

Previous studies of fracture dynamics in graphene have focused on in-plane fracture, also called fracture Mode I, Fig. 3.2a [30, 37, 38, 62], and tearing of graphene nanoribbons, Fig. 3.2b [27, 57].

Here we show that out-of-plane forces can cause free-standing graphene to fracture. This fracture mode is known as the tearing mode and is common in materials such as paper. We present a numerical study of the propagation of cracks in clamped, free-standing graphene as a function of the out-of-plane

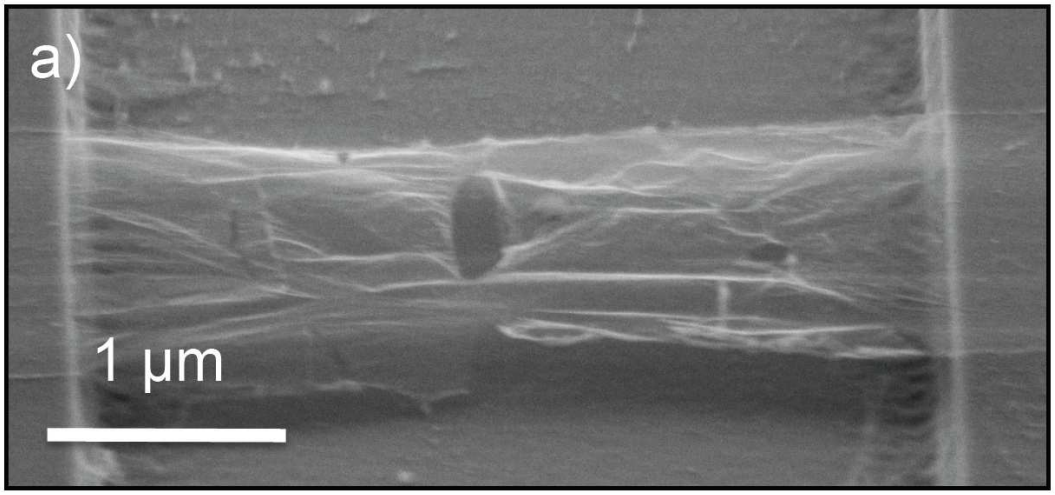

Figure 3.1: Image from [67]: SEM imagine of free-standing graphene membrane with partial tears in the surface.

force. We also obtain an analytical expression for the the minimum force required to tear a two dimensional sheet, such as graphene, in terms of the initial crack length.

Part of the work presented in the chapter was published was in the paper "Tearing graphene" [46]. We are currently writing a paper on the latest simulations and the improved theory.

3.2 Analytical approach to tearing a two dimensional sheet

The system of interest is a two dimensional sheet, such as graphene, with an initial crack of length l. The sheet is suspended and exposed to a uniform downward force f. The problem is to describe the propagation of a

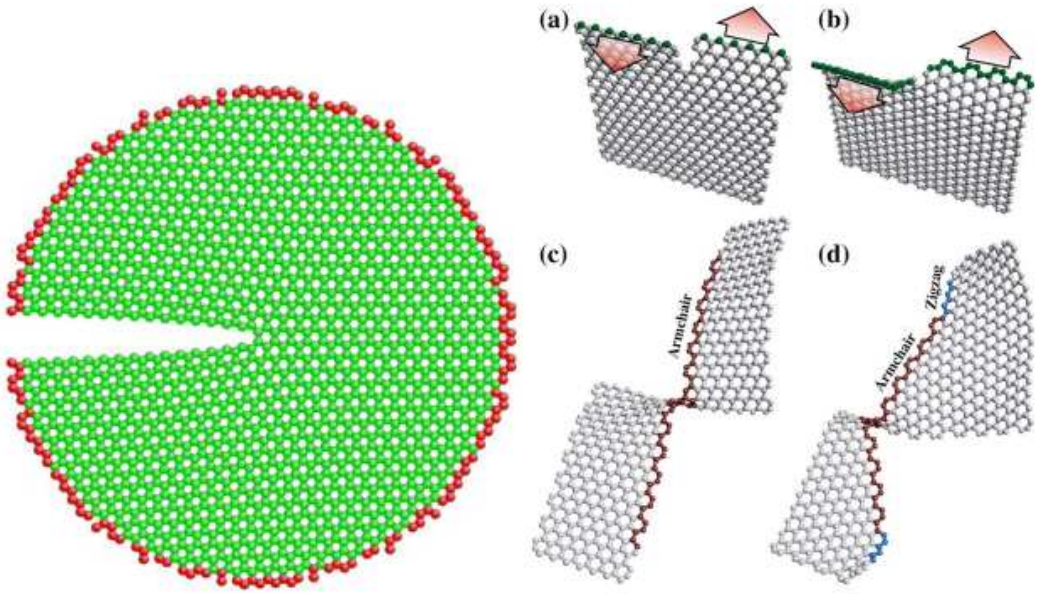

(a) in-plane tearing of graphene sheet (b) tearing of graphene nanoribbons

Figure 3.2: Fig. 3.2a image from [62]: Mode I fracture in a monolayer graphene. Atoms at the outer boundary (red) are fixed, while the remaining atoms (green) are free. Fig. 3.2b image from [27]: Tearing of graphene nanoribbons (along the armchair and the zigzag directions).

crack in such sheet and the minimum force required for the crack to run.

Here we follow a procedure similar to the one developed by Marder [41] for the propagation of a crack in a 3D strip, making the appropriate changes for our two dimensional problem.

Consider a system with an initial crack of length l and total energy $U_{tot}(l)$, Fig. 3.3. The crack can run a length dl if doing so reduces the total energy of the system, that is:

$$U_{tot}(l) > U_{tot}(l + dl) \tag{3.1}$$

The total energy of the system can be written as the energy contained within the crack tip region plus the energy outside of it, U_{out}. The energy to move the crack tip (region) is proportional to the energy of the new surface opened up by the crack. Therefore the total energy of a 2D sheet, such as graphene, with a crack of length l is given by:

$$U_{tot}(l) = \Gamma l + U_{out}(l) \tag{3.2}$$

where Γ is the surface energy density. The surface energy density is material-dependent, and it can be measured experimentally (and obtained numerically).

From Eqs. (3.1) and (3.2) we get Griffith's criterion for a crack to propagate in a 2D sheet:

$$\frac{dU_{out}}{dl} + \Gamma < 0 \tag{3.3}$$

The energy outside the crack tip, U_{out}, depends on the geometry of the system.

Figure 3.3: Top image: Clamped, free-standing two dimensional sheet with an initial crack of length l at the right hand side. Bottom image: Because of an external downward force the crack runs, a length dl, and the sheet bends diagonally.

Cracks on graphene sheets have been observed to come in multiple sizes and shapes [67]. It is intuitive that the force required for a crack to run will depend on the initial crack length. For sheets of paper, for example, it is easier to tear a sheet with a long crack, than to tear one with a short crack. Most experiments focus on electronic properties, and do not look at initial cracks on the samples. Consequently, the shapes of the cracks are in general unknown.

As the exact shape of the cracks is unknown, for simplicity we considered two possible initial conditions: a crack at the very edge of the sheet and a crack in the middle of the sheet.

3.3 Sheet with an edge crack

3.3.1 Analytical study of a sheet with an edge crack

Considering that defects can occur where the graphene sheet meets the support that suspends it we decided to use a crack at the edge of the sheet as our first initial condition.

For an initial crack at the edge of the sheet the downward force will then tear the sheet at the edge making it bend diagonally, as seen on Fig. 3.3. The energy outside the crack tip, U_{out}, is then equivalent to the energy required to bend a 2D sheet.

First, we consider the 1D case of a bending strip (see Fig. 3.4). Then we extend it to the 2D case of a bending sheet.

The energy of a 1D strip of length L under a downward force f is given

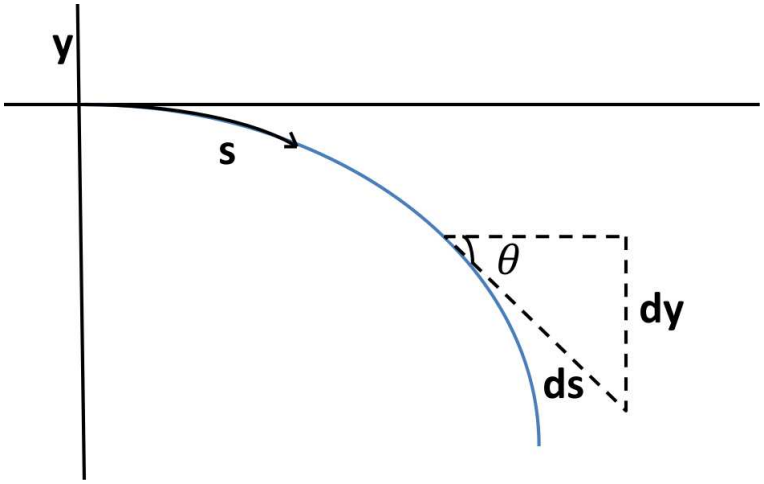

Figure 3.4: One dimensional strip of length L, fixed at one end, and bending due to an external downward force.

by:

$$U_{bend}^{1D} = \int_0^L ds \left[\frac{k_l}{2} \left(\frac{d\theta}{ds} \right)^2 + f_l \cdot y(s) \right] \tag{3.4}$$

where k_l is the bending modulus (times length). The θ term refers to the bending energy and the f_l term refers to energy due to the external downward force (per length) applied to the strip.

The same idea applies to bending a two dimensional sheet, with the difference that now it is a triangle that bends, not just a line (see Fig. 3.5 and 3.6). The area that is free to bend depends on the crack length. Here we assume that U_{out} comes from the bending of a squared sheet of side of length l, which is the crack length (see Fig. 3.5). The energy of a 2D sheet of diagonal

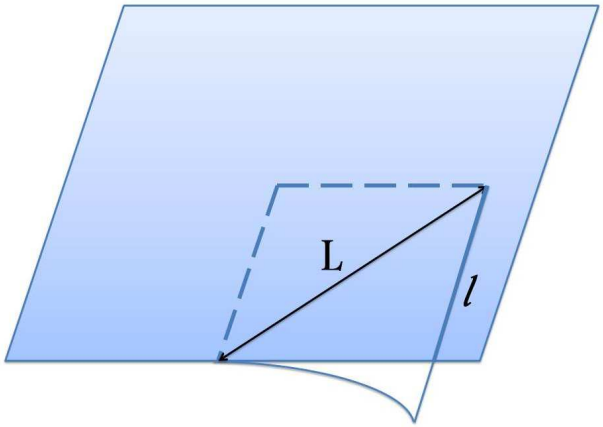

Figure 3.5: Clamped, free-standing two dimensional sheet with an initial crack of length l. The dashed square is the part of the sheet that is initially free-to bend, as it is not attached to the support. The sheet bends because of the applied downward force.

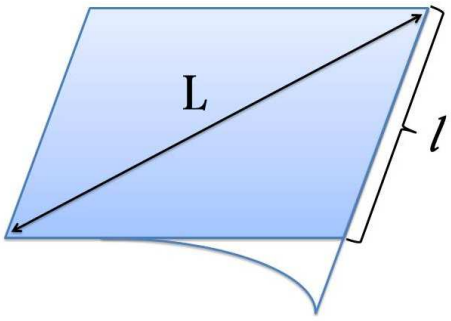

Figure 3.6: Zooming on Fig. 3.5: two dimensional sheet of sides of length l and diagonal length L. The sheet bends because of the applied downward force.

length $L = l\sqrt{2}$ under a downward force f is given by:

$$U_{bend}^{2D} = \int_0^L ds \left[\frac{k}{2} \left(\frac{d\theta}{ds} \right)^2 + f_a \cdot y(s) \right] (L - s), \tag{3.5}$$

where f_a is the external downward force per area applied to the sheet and k is the bending modulus.

From Fig. 3.4 we observe that:

$$\sin(\theta) = \frac{dy}{ds} \tag{3.6}$$

Therefore the downward displacement, both for the 1D and the 2D cases, is given by:

$$y(s) = \int \sin(\theta) ds \tag{3.7}$$

3.3.1.1 Small bending approximation

In our first approach, we use the small bending approximation:

$$\frac{d\theta}{ds} \approx \frac{d^2y}{ds^2} \tag{3.8}$$

Therefore, from Eq. (3.5) and (3.8), we obtain:

$$U_{out} = U_{bend}^{2D} = \int_0^L ds \left[\frac{k}{2} \left(\frac{d^2y}{ds^2} \right)^2 + f_a \cdot y(s) \right] (L - s) \tag{3.9}$$

Minimizing Eq. (3.9) gives us the energy outside the crack tip in terms of the minimum force required for the crack to run. To do so we need to solve the Euler-Lagrange equations for U_{out}:

$$\frac{dU_{out}}{dy} - \frac{d}{ds} \left(\frac{dU_{out}}{dy'} \right) + \frac{d^2}{ds^2} \left(\frac{dU_{out}}{dy''} \right) = 0 \tag{3.10}$$

where $y' = dy/ds$. From that we obtain:

$$f_a(L-s) + k\left[(L-s)\frac{d^4y}{ds^4} - 2\frac{d^3y}{ds^3}\right] = 0 \tag{3.11}$$

Applying the conditions:

1.
$$y(0) = 0$$

2.
$$\frac{dy}{ds}(0) = 0$$

We find the expression for the energy outside the crack tip in terms of the minimum force required for the crack to run:

$$U_{out}^{edge} = -\frac{f_a^2 L^6}{432k} = -\frac{f_a^2 l^6}{54k} \tag{3.12}$$

where we used that $L = l\sqrt{2}$. Combining this result with the Griffith's criterion, Eq. (3.3), we obtain the expression that relates the minimum force (per area) required for an edge crack to run on a 2D sheet, f_a, to the initial crack length, l:

$$f_a^{edge} = 3\sqrt{\frac{\Gamma k}{l^5}} \tag{3.13}$$

The bending modulus, k, and the surface energy density, Γ, of graphene can be measured experimentally (and also obtained numerically) [19, 28, 52, 64].

In the next section we will see that this expression does not match our simulations, and it is **incorrect**. In Sec. 3.5 we discuss why the small bending approximation is not appropriate for this problem and we present an improved theory.

3.3.2 Numerical study of a sheet with an edge crack

A similar approach to the simulation of ripples in graphene (Chap. 2) is used to study of the propagation of cracks in clamped, free-standing graphene as a function of the out-of-plane force.

Here we use the MEAM semi-empirical potential [9], shown to reproduce well the properties of graphene [35, 64] and to support crack propagation [25]. The energy minimization is done through damped molecular dynamics. To better model the experimental conditions, all the simulations in this work are of finite-sized graphene sheets, and no periodic boundary conditions are used. These simulations were done at zero temperature, to show only the fracture mechanics of the graphene sheet.

Inspired by the bending of a sheet of paper (Fig. 3.3, top image) we wrote the initial shape of the graphene sheet with a crack at the edge in terms of exponential functions. We start with a flat graphene sheet, where the position of the atom i is represented by (x_0^i, y_0^i, z_0^i). Now consider a straight crack that runs parallel to the x-axis and has a length of x_{cut}. To open the crack we keep the x and y position of the atom and change z by:

$$z^i = z_0^i - P_A \left(1 - \exp\left(P_B \cdot y_0^i\right)\right) \cdot \left(1 - \exp\left(P_B(-x_0^i + x_{cut})\right)\right) \qquad (3.14)$$

Figure 3.7: Initial edge crack of $l \approx 10$Å in a 100Å by 100Å clamped, free-standing graphene sheet.

Figure 3.8: Constant downward force is applied on the sheet of Fig. 3.7. Initially the sheet wrinkles and bends.

The parameters P_A and P_B determine the curvature of the sheet.

As an example of an initial condition, Fig. 3.7 shows a crack of $l \approx 10$Å at the edge of a suspended graphene sheet. The clamped edges are not allowed to move and where chosen to have a width of ≈ 5Å. A uniform downward force is then applied to every atom on the sheet. Once sufficient force is applied, the crack starts running, as seen on Fig. 3.9. We have also made videos of crack propagations. Appendix D has a link to some movies.

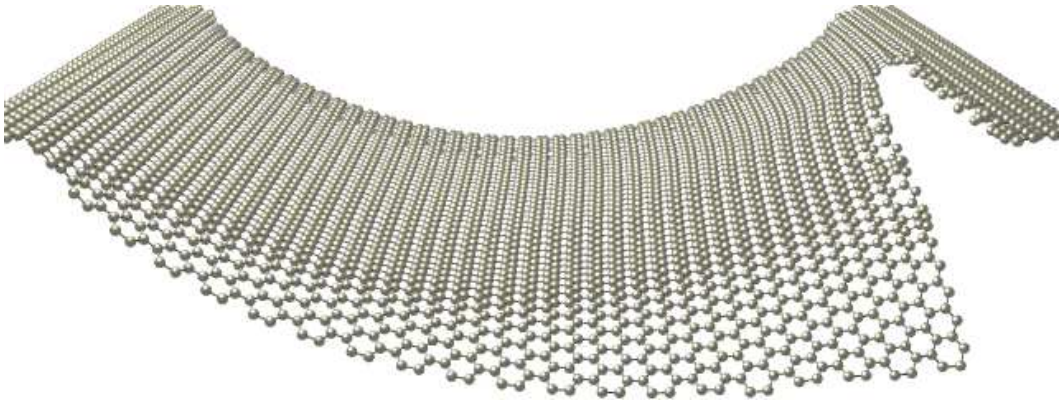

Figure 3.9: Downward constant force is applied on the sheet of Fig. 3.7. After the sheet wrinkles and bends the crack propagates.

The simulations show that, depending on the initial condition, a crack will not run straight through the sheet, as initially expected (see Fig. 3.10 and Fig. 3.11). Short initial cracks run straight, while longer cracks do not. It could be useful to find the threshold value of the initial crack length that determines the dynamics of the crack propagation.

Another interesting result is that, depending on the initial crack length and orientation (zigzag or armchair), the propagation pattern will be different (see Fig. 3.10 and Fig. 3.11). Similar dynamics have been seen in simulations of tearing graphene nanoribbons [27]. The edge orientation of a graphene nanoribbon can determine its electronic properties. Therefore it would be most useful to be able to predict the edge orientation of produced samples.

In our simulations we noticed that if the initial crack is not sufficiently open, it closes on its own (the sheet "heals"). While this is contrary to daily experience, it is possible with quantum mechanical objects, which we model

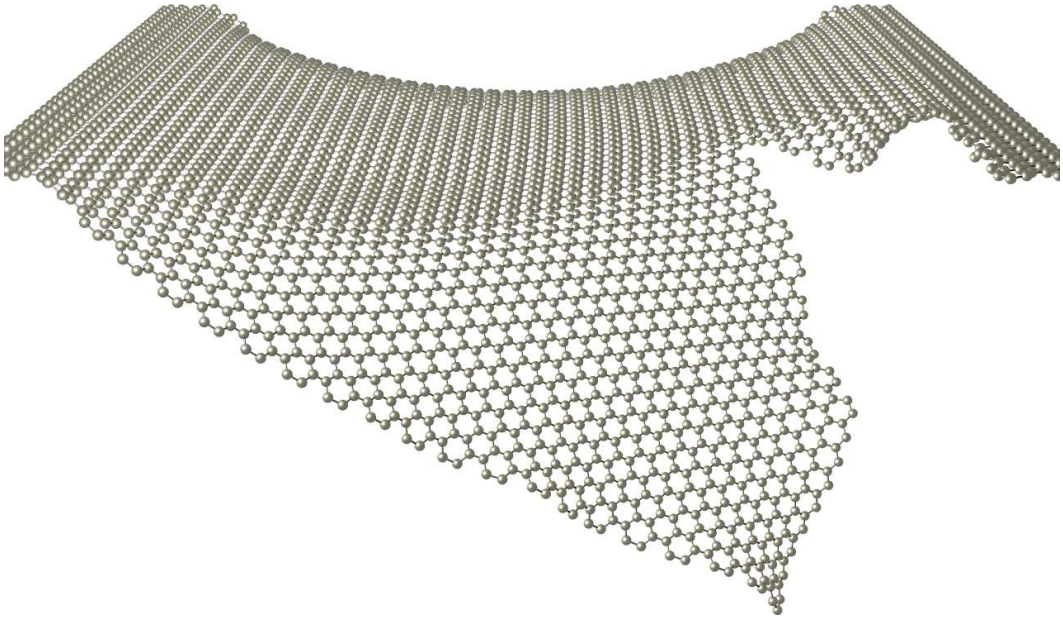

Figure 3.10: Non-straight crack propagation in a 100Å by 100Å graphene sheet with an initial crack of $l \approx 25$Å. Note that the initial zigzag crack propagates as armchair.

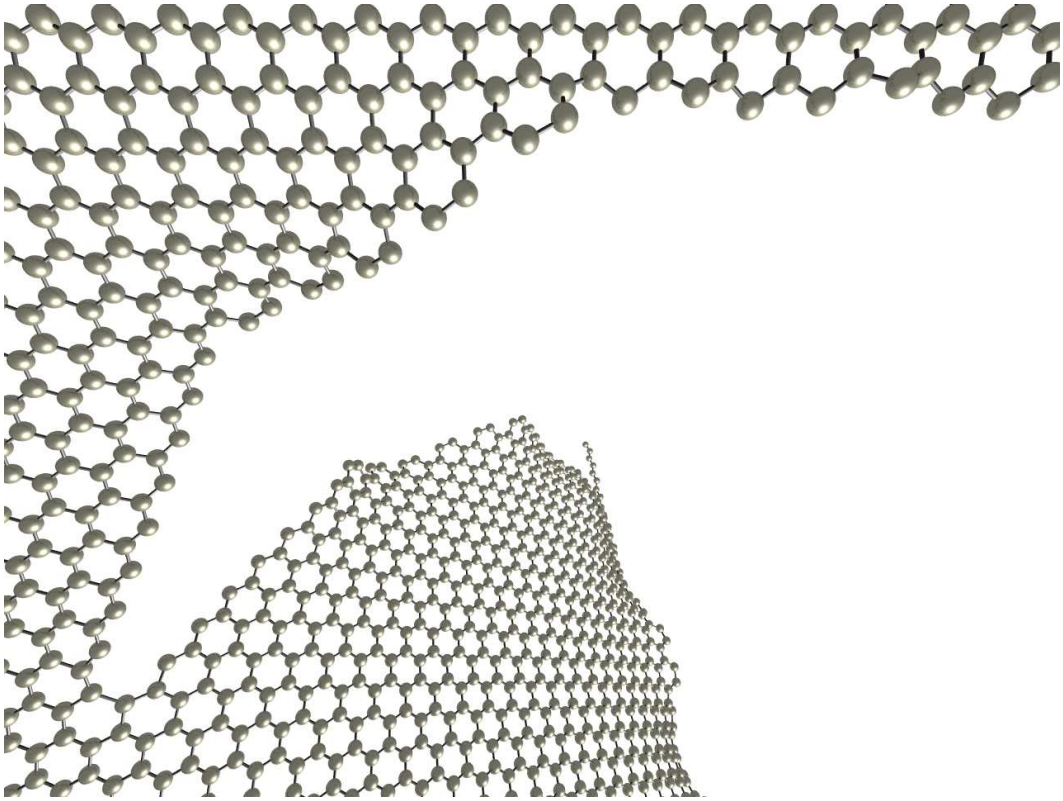

Figure 3.11: Non-straight crack propagation in a 100Å by 100Å graphene sheet with an initial crack of $l \approx 30$Å. Note that the initial zigzag crack propagates as armchair and then turns zigzag again.

with a semi-empirical potential that combines attractive and repulsive forces. We do not know what creates cracks in graphene sheets in these experiments, or what keeps them open. It could be impurities, defects, or something else in the experimental setup. In the theory of fracture mechanics, Section 3.2, crack propagation is independent of the mechanism that initially creates the crack. For this study, therefore, we choose our initial conditions such that the crack is kept open.

Another issue we encountered is determining the period of time that it takes for a crack to begin to run. The simulations show that first the sheet ripples and bends, and then the crack runs. In terms of energy, what we see is an initial large drop in potential and kinetic energy, Fig. 3.12. Then the sheet reaches an almost-stable state, where the energy almost plateaus, decreasing very slowly. Finally, when the crack runs, another drop in potential energy occurs together with a fast increase in kinetic energy. If the force applied is not strong enough for the crack to run, the sheet stays in the bent state forever. Numerically we have to set an acceptable period of time to be considered "forever". We observe that longer initial crack lengths lead to longer periods of time spent in the almost-stable state. After studying many simulations we decided that 600,000 time steps is, in most cases, an acceptable period of time to study the crack propagation (or lack of it).

To compare the numerical results with the analytical expression, Eq. (3.13), we need the values of the bending modulus k and the surface energy density Γ for graphene.

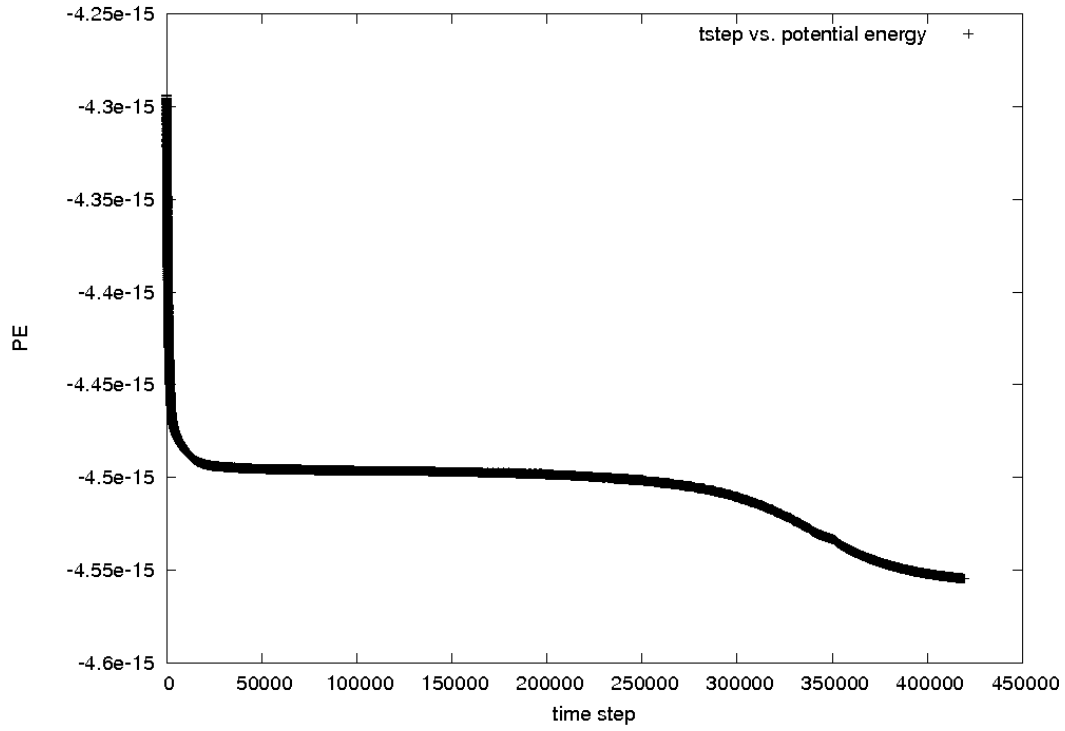

Figure 3.12: Graph of potential energy (in Joules) vs time step for an initial edge crack of $l \approx 35$Å. The first large drop in potential energy happens while the sheet ripples and bends. Then potential energy slowly decreases as the ripples disappear and the sheet reaches its fully bent state. Another fast drop in potential energy occurs when the crack starts running.

The experimental value of the bending modulus of graphene is [52]:

$$k_{exp} = 1.2\text{eV} \approx 1.92 \times 10^{-19}\text{J} \tag{3.15}$$

From our previous numerical work on ripples in graphene we found $k = 1.77$eV [64]. Another numerical study, by Fasolino *et al.* [19], obtained $k = 1.1$eV.

We have not been able to find an experimental measurement of the surface energy density of graphene in the literature. From our simulations we obtained:

$$\Gamma_{numerical} \approx 3.82 \times 10^{-9}\text{J/m} \tag{3.16}$$

For the full numerical calculation of graphene's surface energy see Appendix C.

The uniform downward force is applied to every atom on the sheet, therefore numerically we use force per atom f_{atom}, and not force per area f_a, as derived in the analytical calculations. For graphene the number of atoms per area is:

$$\eta = 38.17 \times 10^{18}\text{m}^{-2} \tag{3.17}$$

So, the relationship between force per atom and force per area is:

$$f_{atom} = \frac{f_a}{\eta} = \frac{f_a}{38.17 \times 10^{18}\text{m}^{-2}} \tag{3.18}$$

Fig. 3.13 shows a graph of force per atom versus initial crack length. The line is the theoretical expression, Eq. (3.13), and the plus symbols are the

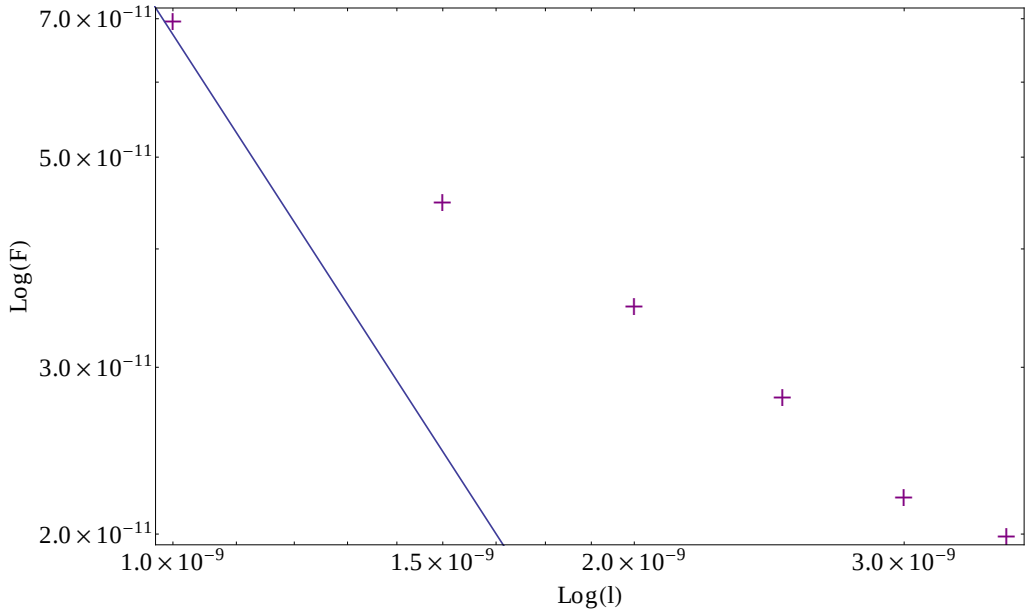

Figure 3.13: Log-log graph of force (in Newtons per atom) vs initial crack length (in meters) for an edge crack. The line is the theoretical expression, Eq. (3.13), and the plus symbols are the numerical results.

numerical results. Note that these are approximate crack lengths. The crack length is not well defined, because the crack tip is not well defined.

Numerically we observed that as the initial crack length gets bigger the crack does not run straight, which could explain the disagreement between numerical and analytical calculations, as the analytical calculation does not account for this type of crack dynamics. Another behavior that is different in the analytical and numerical studies is that numerically the sheet first wrinkles and bends, see Fig. 3.8, and then the crack runs. This is also not accounted for in the analytical study.

In order to see if we could change the crack propagation pattern we decided to ignite the crack tip, that is, give the atoms at the crack tip a small downward velocity. We performed this test for multiple initial crack lengths and it resulted in the same unpredictable crack propagation seen before.

The inconsistency of the crack propagation and the lack of agreement with the theory motivated us to try a more symmetric initial condition - a sheet with a crack in the middle.

3.4 Sheet with a crack in the middle

3.4.1 Analytical study of a sheet with a crack in the middle

A sheet with an initial crack in the middle is equivalent to two sheets with an edge crack, which is the problem we just solved in the previous section. Therefore:

$$U_{out}^{middle} = 2U_{out}^{edge} \tag{3.19}$$

Following from our result considering the small bending approximation, Eq. (3.12):

$$U_{out}^{middle} = -\frac{f_a^2 l^6}{27k} \tag{3.20}$$

Again using this result with Griffith's criterion, Eq. (3.3), we now obtain an expression that relates the minimum force (per area) required for a crack to run in the middle of a 2D sheet to the initial crack length, l:

$$f_a^{middle} = 3\sqrt{\frac{\Gamma k}{2l^5}} \tag{3.21}$$

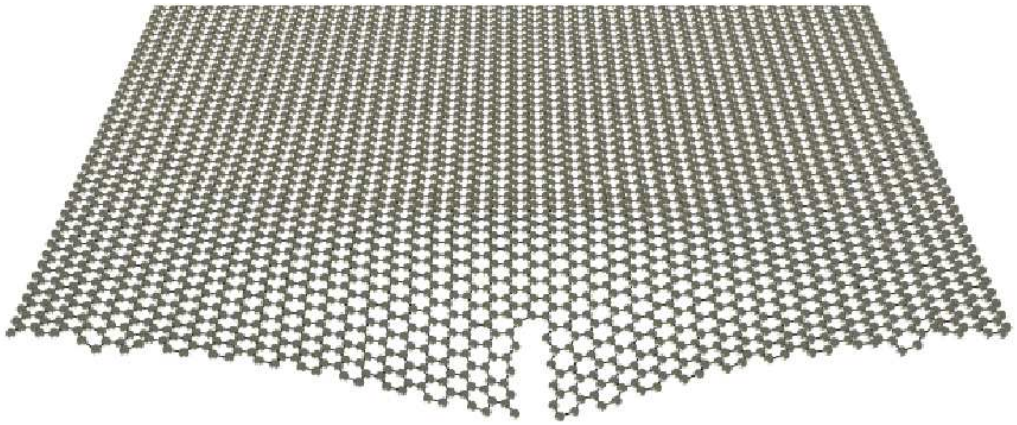

Figure 3.14: Initial crack of ≈ 10Å in length and ≈ 2Å in width in a 100Å by 100Å clamped, free-standing graphene sheet.

Once again, we will see that this expression does not match our simulations, and it is **incorrect**. In Sec. 3.5 we discuss why the small bending approximation is not appropriate for this problem and we present an improved theory.

3.4.2 Numerical study of a sheet with a crack in the middle

3.4.2.1 Crack in the middle of the sheet generated by defects

As explained on Sec. 3.3.2, in our simulations if the initial crack is not sufficiently open, it closes on its own. In order to have a clean open crack in the middle of the graphene sheet we simulated a sheets with defects, lacking of a line of atoms. We also bent the sheet on both sides of the crack using a variation of Eq. (3.14). A sheet with an initial crack of $l \approx 10$Å produced by the procedure just described is shown in Fig. 3.14. Cracks produced by these

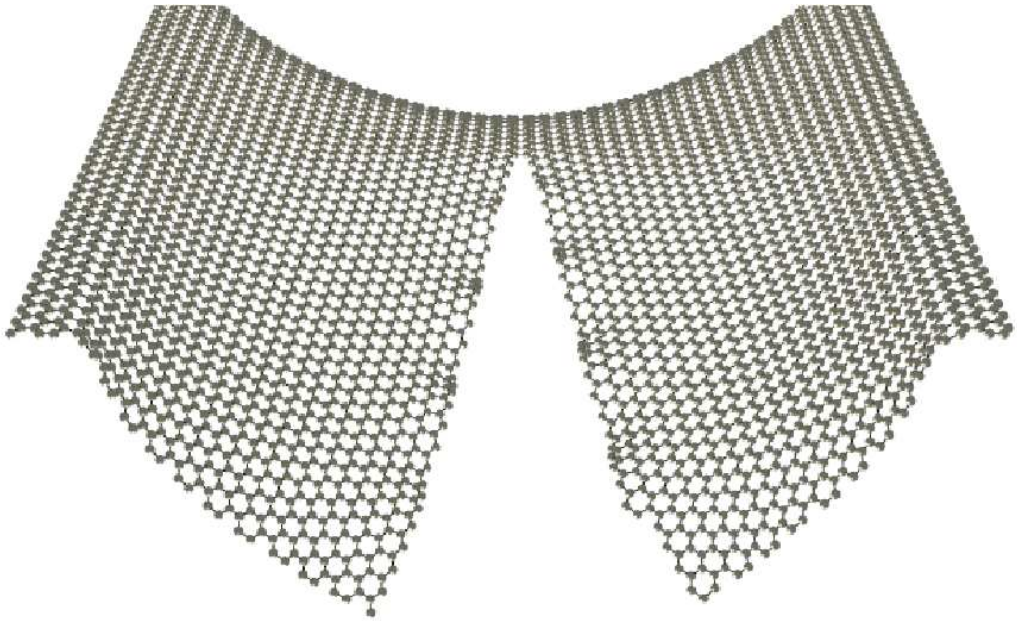

Figure 3.15: A uniform constant downward force is applied on the sheet of Fig. 3.14. First the sheet wrinkles and bends and then the crack propagates.

defects were observed consistently to run straight, as seen on Fig. 3.15.

Fig. 3.16 shows a graph of the numerical results and the analytical expression, Eq. (3.21). Even though these simulations do not exhibit crack propagation pattern issues, again theoretical and numerical results do not agree. More importantly, the defects (lack of atoms) can generate blunt crack tips, which in turn might require a higher force for the crack to propagate. These concerns motivated us to develop another method to simulate cracks in the middle of graphene sheets.

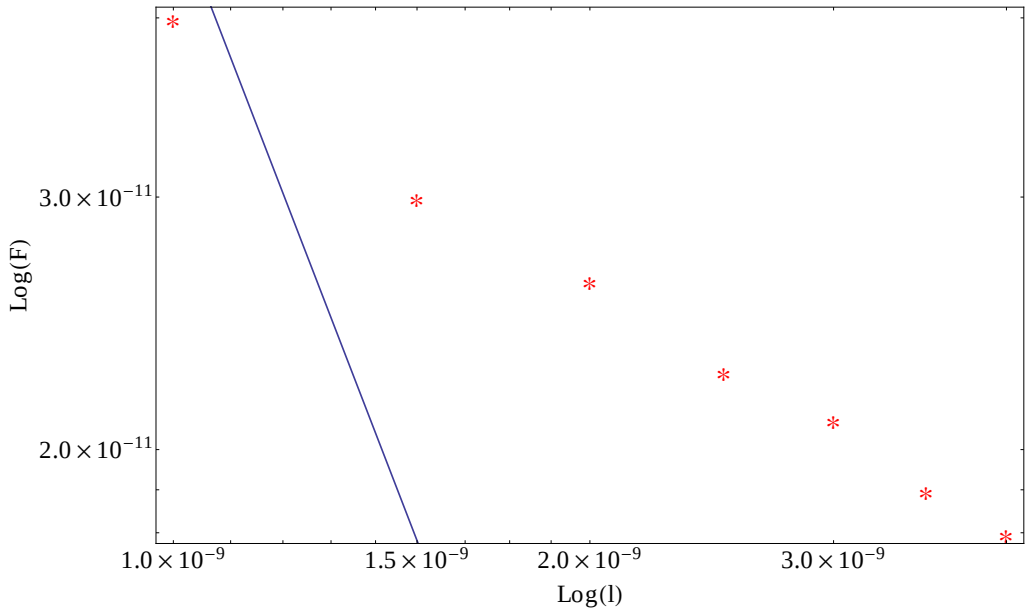

Figure 3.16: Log-log graph of force (in Newtons per atom) vs initial crack length (in meters) for a sheet that exhibits defects. The line is the theoretical expression Eq. (3.21), and the stars are the numerical results.

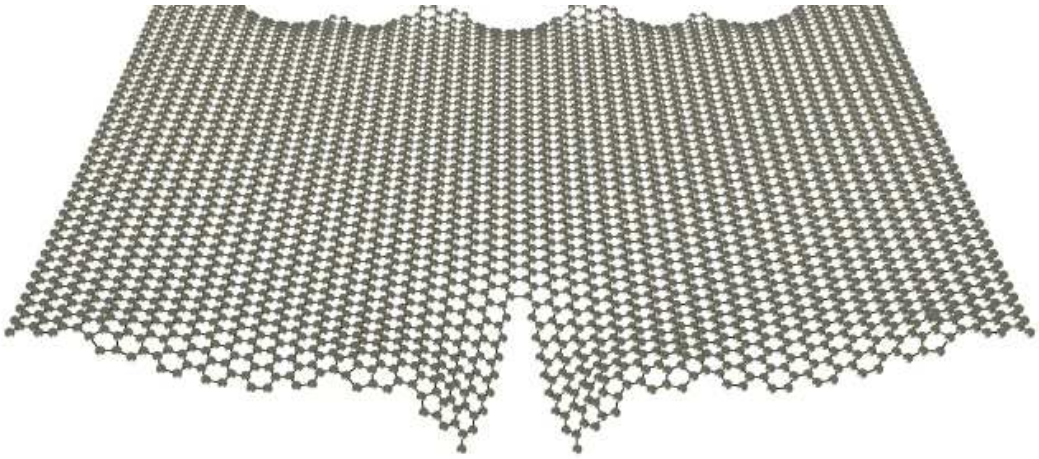

Figure 3.17: Initial crack of $l \approx 25$Å generated by an opening of $\approx 20°$ in a 100Å by 100Å clamped, free-standing graphene sheet.

3.4.2.2 Crack in the middle of the sheet generated by a wide opening

To generate a clean open crack with a sharp crack tip we created a wide opening in the middle of the graphene sheet. In fracture mechanics this is called a Mode I crack, or opening mode. Along with the opening, we also bent the sheet on both sides of the crack using a variation of Eq. (3.14). A sheet with an initial crack of $l \approx 25$Å generated by the opening and bending method just discussed is shown in Fig. 3.17 Cracks produced by this method were observed consistently to run straight (see Fig. 3.18).

Fig. 3.19 shows a log-log graph of the numerical results and the analytical expression, Eq. (3.21). Fig. 3.20 shows graphs of force versus initial crack length. The line is the theoretical expression Eq. (3.21), the dots are the numerical results for an opening in the middle of the sheet, and the stars are the

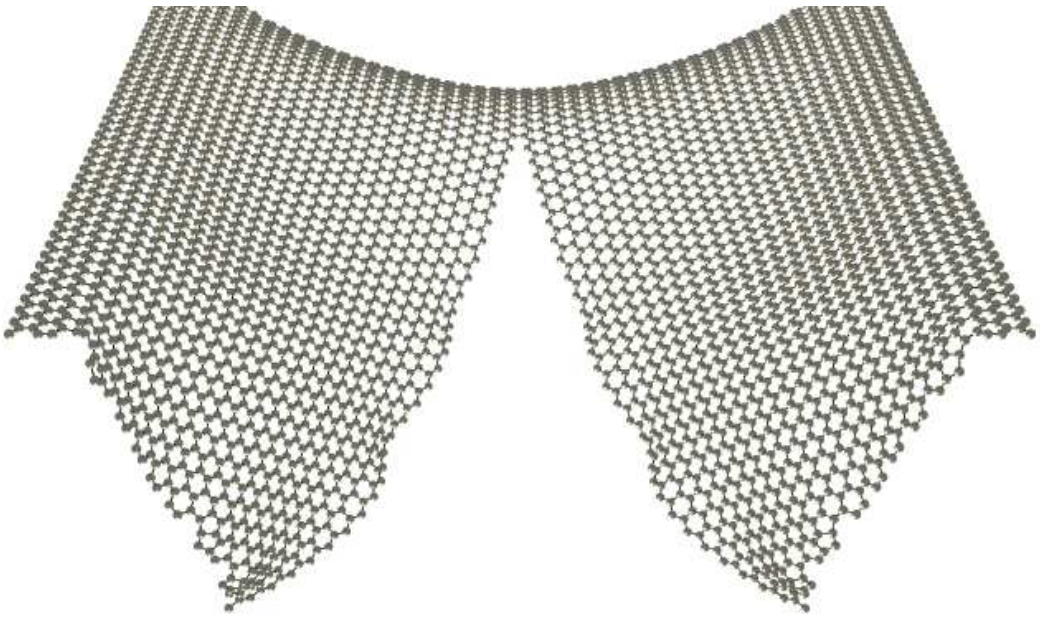

Figure 3.18: A uniform constant downward force is applied on the sheet of Fig. 3.17 and the crack propagates.

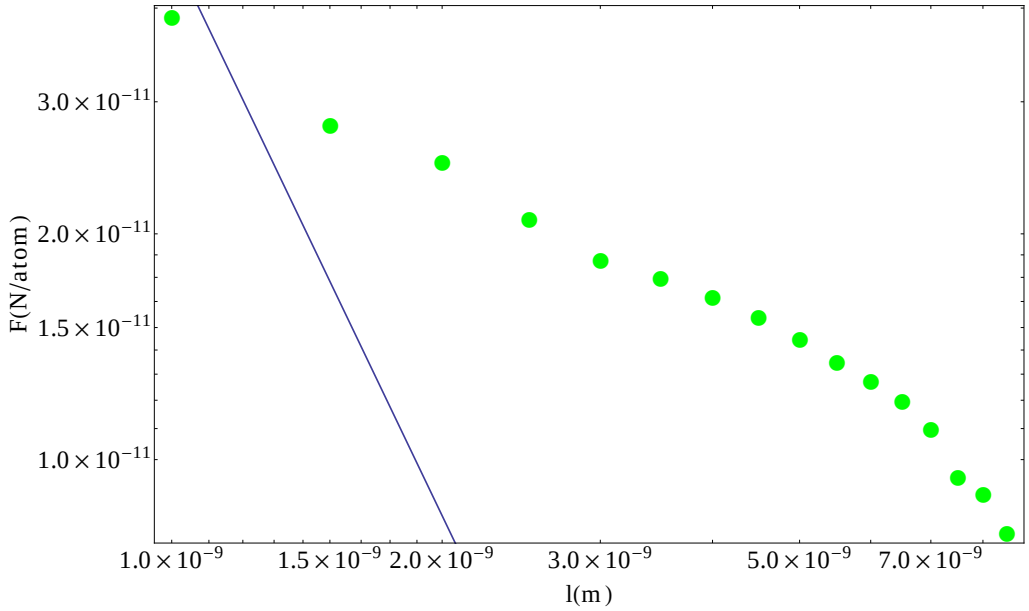

Figure 3.19: Log-log graph of force (in Newtons per atom) vs initial crack length (in meters) for a wide-open middle crack. The line is the theoretical expression, Eq. (3.21), and the dots are the numerical results.

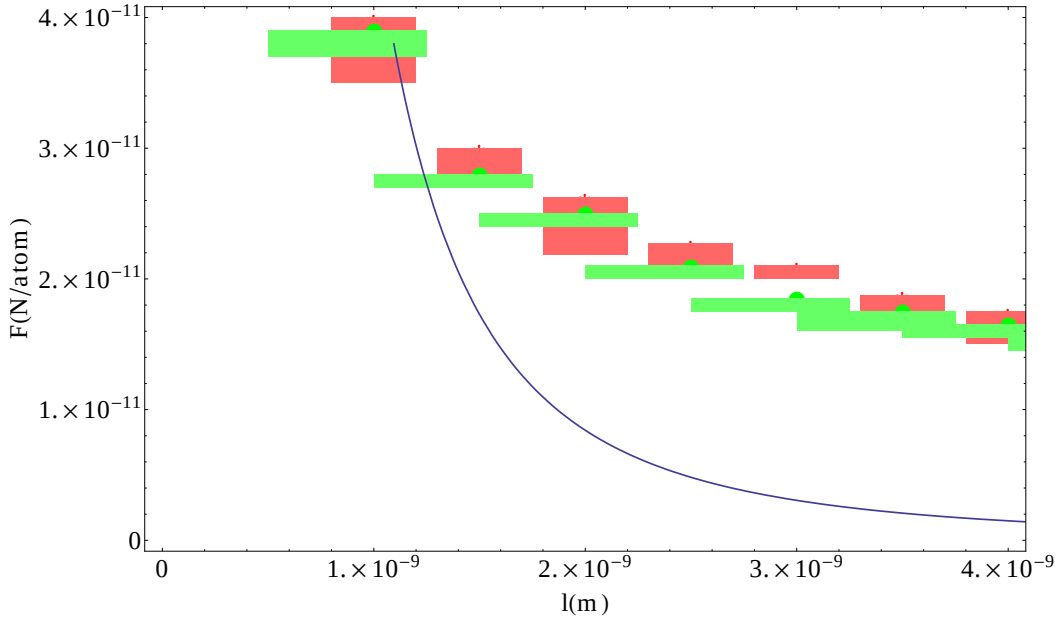

Figure 3.20: Graph of force (in Newtons per atom) vs initial crack length (in meters) . The line is the theoretical expression, Eq. (3.21), the green dots are the numerical results for a wide-open middle crack and the red stars are the numerical results for a sheet that exhibits defects.

numerical results for a sheet that exhibits defects (see previous section). The horizontal error bars are estimated uncertainties of the initial crack length due to the fact that the crack tip is not well defined. The vertical error bars are due to the precision of our numerical simulations. Note that for approximately the same initial crack length a crack generated by defects (a missing line of atoms) and a crack generated by an opening, run at a about the force.

Both methods to generate cracks in the middle of the sheet, by defect or wide opening, show a straight crack propagation pattern. This is different from the edge crack propagation. The theoretical expressions seem to under

estimate the force required for a crack to run for all the initial scenarios presented (edge crack, crack in the middle of the sheet generated by defects, and crack in the middle of the sheet generated by a wide opening).

3.5 Improved theory - crease energy

Because of the lack of agreement between the theory and the multiple numerical results we decided to derive a new theory for the energy required to bend a 2D sheet. First we will go back to the analytical calculations, Sec. 3.3.1, and find the energy outside the crack tip without considering the small bending approximation. Second, from the numerical simulations we noticed that the sheet folds in a crease (on both sides of the crack) before the crack runs, Fig. 3.21. To take this behavior into account we will consider the sheet folding from the crack tip all the way to the fixed end, instead of the bending in half a square, as proposed in Sec. 3.3.1. In experiments, folds, scrolls, and creases are commonly observed in free-standing graphene samples.

As before, we will start considering the 1D case of a bending strip (see Fig. 3.4). Then we will extend it to the 2D case of a bending sheet.

3.5.1 Energy for a bending strip (no small bending approximation)

Here we obtain the energy to bend a 1D strip not assuming the small bending approximation. We observed that the sheets folds in a crease, as explained above, consequently this approximation does not apply.

The energy of a 1D strip of length L under a downward force f_l is given

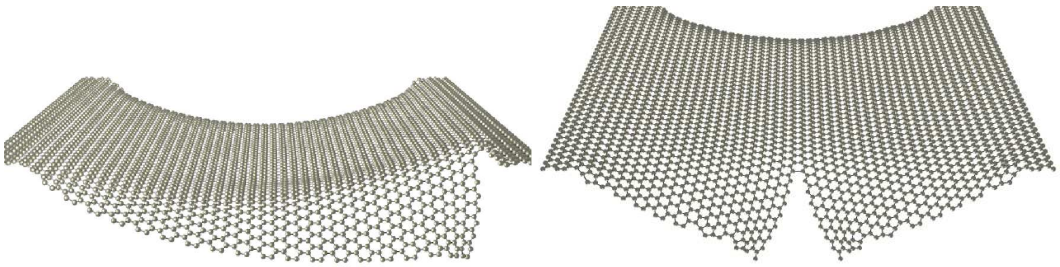

(a) initial edge crack of $l \approx 20$Å (b) initial middle crack of $l \approx 25$Å

Figure 3.21: Clamped, free-standing graphene sheets with an initial crack (at the edge and in the middle) under a downward constant force. In both cases the sheet exhibits a crease before the crack runs. The crease goes from the crack tip basically all the way to the fixed end.

by (Eqs. (3.4) and (3.7)):

$$U_{bend}^{1D} = \int_0^L ds \left[\frac{k_l}{2} \left(\frac{d\theta}{ds} \right)^2 + f_l \int_0^s \sin(\theta(s'))ds' \right] \tag{3.22}$$

Note that s' is just a variable (**not** a derivative of s).

As before, we need to minimize Eq. (3.22) to obtain the energy outside the crack tip in terms of the minimum force required for the crack to run. To find the minimum (or the maximum) of U_{bend}^{1D} we take the functional derivative and make it equal to zero:

$$\lim_{\epsilon->0} \frac{U_{bend}^{1D}(\theta + \epsilon\phi) - U_{bend}^{1D}(\theta)}{\epsilon} = 0 \tag{3.23}$$

This results in:

$$\lim_{\epsilon->0} \frac{1}{\epsilon} \int_0^L ds \left\{ \frac{k_l}{2} \left[2\epsilon \frac{d\phi}{ds}\frac{d\theta}{ds} + \epsilon^2 \left(\frac{d\phi}{ds} \right)^2 \right] + f_l \int_0^s \left[\sin(\theta(s') + \epsilon\phi(s')) - \sin(\theta(s')) \right] ds' \right\} = 0 \tag{3.24}$$

Expanding the sine function in a Taylor series we obtain:

$$\lim_{\epsilon->0} \frac{1}{\epsilon} \int_0^L ds \left\{ \frac{k_l}{2} \left[2\epsilon \frac{d\phi}{ds} \frac{d\theta}{ds} + \epsilon^2 \left(\frac{d\phi}{ds} \right)^2 \right] + f_l \int_0^s \left[\epsilon\phi(s') \cos(\theta(s')) + O(\epsilon^2) \right] ds' \right\} = 0 \tag{3.25}$$

Dividing by ϵ and taking the limit as it goes to zero:

$$\int_0^L ds \left\{ \frac{k_l}{2} 2 \frac{d\phi}{ds} \frac{d\theta}{ds} + f_l \int_0^s \phi(s') \cos(\theta(s')) ds' \right\} = 0 \tag{3.26}$$

Using integration by parts on the first term and the fact that ϕ vanishes at 0 and L:

$$\int_0^L ds \left\{ -k_l \phi \frac{d^2\theta}{ds^2} + f_l \int_0^s \phi(s') \cos(\theta(s')) ds' \right\} = 0 \tag{3.27}$$

The result should be independent of the test function ϕ. Here we choose $\phi = \delta(s - s'')$:

$$\int_0^L ds \left\{ -k_l \delta(s - s'') \frac{d^2\theta}{ds^2} + f_l \int_0^s \delta(s' - s'') \cos(\theta(s')) ds' \right\} = 0 \tag{3.28}$$

After some algebra we obtain:

$$-k_l \frac{d^2\theta(s'')}{ds''^2} + f_l \cos(\theta(s''))(L - s'') = 0 \tag{3.29}$$

Note that s'' is just a variable (**not** the second derivative of s).

At this point an appropriate approximation needs to be considered in order to solve this equation analytically.

3.5.2 One-dimensional crease energy

Here we consider the limit $L \to \infty$, since by the time s'' is comparable to L, $\theta = -\pi/2$. Eq. (3.29) then simplifies to:

$$-k_l \frac{d^2\theta(s'')}{ds''^2} + f_l \cos(\theta(s''))L = 0 \tag{3.30}$$

After some manipulation we obtain:

$$\frac{d\theta(s'')}{ds''} = \sqrt{2\frac{f_l L}{k_l}\sin(\theta(s'')) - C_1} \tag{3.31}$$

where C_1 is a constant, and it can be determined from the following conditions:

1.
$$\frac{d\theta}{ds''}(L) = 0$$

2.
$$s'' \to L, \theta \to -\frac{\pi}{2}$$

The result is:

$$C_1 = 2\frac{f_l L}{k_l}\sin(\theta(L)) = 2\frac{f_l L}{k_l}\sin\left(-\frac{\pi}{2}\right) = -2\frac{f_l L}{k_l} \tag{3.32}$$

Plugging it back into Eq. (3.31):

$$\frac{d\theta(s'')}{ds''} = \sqrt{2\frac{f_l L}{k_l}\left[\sin(\theta(s'')) + 1\right]} \tag{3.33}$$

Substituting:

$$\theta(s'') = \frac{\pi}{2} - \Phi(s'') \tag{3.34}$$

and using the trigonometric identities:

1. $\sin(\frac{\pi}{2} - \Phi) = \cos(\Phi)$

2. $\cos(\Phi) + 1 = 2\cos^2(\Phi/2)$

we obtain:

$$\frac{d\Phi(s'')}{ds''} = -2\sqrt{\frac{f_l L}{k_l}}\cos(\Phi(s'')/2) \tag{3.35}$$

After some manipulation that results in:

$$\Phi(s'') = 2\arccos\left(\operatorname{sech}\left(\sqrt{\frac{f_l L}{k_l}}s'' - C_2\right)\right) \tag{3.36}$$

where C_2 is a constant to be determined.

Using Eq. (3.34) we can go back to θ:

$$\theta(s'') = \frac{\pi}{2} - 2\arccos\left(\operatorname{sech}\left(\sqrt{\frac{f_l L}{k_l}}s'' - C_2\right)\right) \tag{3.37}$$

Applying the condition that $\theta(0) = 0$, we obtain the expression for the bending function of a 1D strip:

$$\theta(s'') = \frac{\pi}{2} - 2\arccos\left(\operatorname{sech}\left(\sqrt{\frac{f_l L}{k_l}}s'' + \operatorname{arccosh}\left(\sqrt{2}\right)\right)\right) \tag{3.38}$$

Now that we have θ we can plug it back in Eq. (3.22) and find:

$$\begin{aligned} U^{1D}_{crease} = -\frac{1}{2}f_l L^2 - 2\sqrt{2}\sqrt{f_l k_l L} \\ +\frac{2k_l}{L}\ln\left[\cosh\left(\sqrt{\frac{f_l L^3}{k_l}}\right) + \frac{1}{\sqrt{2}}\sinh\left(\sqrt{\frac{f_l L^3}{k_l}}\right)\right] \\ +2\sqrt{f_l k_l L}\tanh\left(\sqrt{\frac{f_l L^3}{k_l}} + \operatorname{arccosh}\left(\sqrt{2}\right)\right) \end{aligned} \tag{3.39}$$

Looking at the asymptotic behavior for large L:

$$U^{1D}_{crease} = -\frac{1}{2}f_l L^2 + 2\left(2 - \sqrt{2}\right)\sqrt{f_l k_l L} \tag{3.40}$$

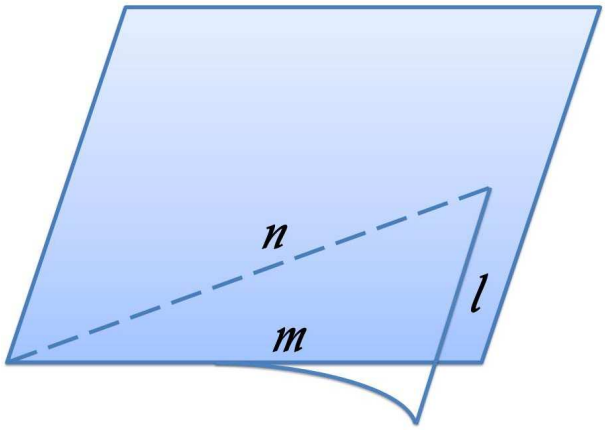

Figure 3.22: Suspended sheet with an initial crack of length l. The triangle formed by the crease is the part of the sheet that is initially free to bend, as it is not attached to the support.

3.5.3 Two-dimensional crease energy

The numerical simulations show that a crease forms (on both sides of the crack) before the crack runs, see Fig. 3.21. Here we present a theory for the sheet folding from the crack tip all the way to the fixed end, Fig. 3.22. Before, in Sec.3.3.1, we considered the bending energy for a square of sides of length l. Now we are considering a right triangle, with one side of length l, the crack length, and another side of length m, the width of the sheet (minus the fixed length, assuming the sheet bends all the way to the fixed end).

In the previous section we obtained the energy of a bending strip under a downward force. We can now integrate that result over the right triangle to obtain the bending energy of a triangle. To be able to perform this integration we need to break the triangle into two parts, see Fig. 3.23. Therefore we

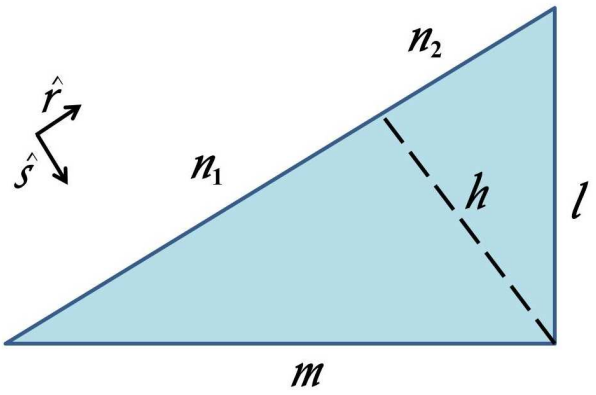

Figure 3.23: Zooming on Fig.3.22: right triangle formed by the crease, $n = n_1 + n_2$, the crack length, l, and the width of the sheet (minus the fixed length), m.

obtain:

$$U^{2D}_{crease} = U_1 + U_2 \tag{3.41}$$

where:

$$U_1 = \int_0^{n_1} dr_1 \int_0^{L(r_1)} ds \left[\frac{k}{2} \left(\frac{d\theta}{ds} \right)^2 + f_a \int_0^s \sin(\theta(s'))ds' \right] \tag{3.42}$$

and

$$U_2 = \int_0^{n_2} dr_2 \int_0^{L(r_2)} ds \left[\frac{k}{2} \left(\frac{d\theta}{ds} \right)^2 + f_a \int_0^s \sin(\theta(s'))ds' \right] \tag{3.43}$$

Notice that, in the two-dimensional case, the total bending length, $L(r)$, varies throughout the triangle, and is written as $L(r_1) = \frac{h}{n_1} r_1$ for the first triangle, and $L(r_2) = \frac{h}{n_2} r_2$ for the second triangle. The height of the triangle is given by $h = \frac{m \cdot l}{\sqrt{m^2+l^2}}$ and the hypotenuse by $n = n_1 + n_2 = \sqrt{m^2 + l^2}$ (see Fig. 3.23).

From the 1D case, Eq. (3.38), we have that the bending function is given by:

$$\theta(s) = \frac{\pi}{2} - 2\arccos\left(\operatorname{sech}\left(\sqrt{\frac{f_a L(r)}{k}}s + \operatorname{arccosh}\left(\sqrt{2}\right)\right)\right) \tag{3.44}$$

First, let us calculate U_1, Eq. (3.42). The integral in s was already solved in the 1D case (Eq. (3.39)):

$$\begin{aligned} U_1 = \int_0^{n_1} dr_1 \Big[&-\frac{1}{2} f_a L^2(r_1) - 2\sqrt{2}\sqrt{f_a k L(r_1)} \\ &+2\frac{k}{L(r_1)} \ln\left(\cosh\left(\sqrt{\frac{f_a}{k}L^3(r_1)}\right) + \frac{1}{\sqrt{2}}\sinh\left(\sqrt{\frac{f_a}{k}L^3(r_1)}\right)\right) \\ &+2\sqrt{f_a k L(r_1)}\tanh\left(\sqrt{\frac{f_a}{k}L^3(r_1)} + \operatorname{arccosh}(\sqrt{2})\right)\Big] \end{aligned} \tag{3.45}$$

The asymptotic behavior for large L, also obtained in our 1D study (Eq. (3.40)), results in:

$$U_1 = \int_0^{n_1} dr_1 \left[-\frac{1}{2} f_a L^2(r_1) + 2\left(2 - \sqrt{2}\right)\sqrt{k f_a L(r_1)}\right] \tag{3.46}$$

Substituting $L(r_1) = h r_1/n_1$:

$$U_1 = \int_0^{n_1} dr_1 \left[-\frac{1}{2} f_a h^2 \frac{r_1^2}{n_1^2} + 2\left(2 - \sqrt{2}\right)\sqrt{k f_a h \frac{r_1}{n_1}}.\right] \tag{3.47}$$

Solving the integral in r_1 we obtain:

$$U_1 = n_1 \left[-\frac{1}{6} f_a h^2 + \frac{4}{3}\left(2 - \sqrt{2}\right)\sqrt{k f_a h}\right] \tag{3.48}$$

As U_2 is analogous to U_1, Eq. (3.41) results in:

$$U^{2D}_{crease} = U_1 + U_2 = (n_1 + n_2)\left[-\frac{1}{6} f_a h^2 + \frac{4}{3}\left(2 - \sqrt{2}\right)\sqrt{k f_a h}\right] \tag{3.49}$$

Substituting $n = n_1 + n_2 = \sqrt{m^2 + l^2}$ and $h = \frac{ml}{\sqrt{m^2+l^2}}$, we obtain that the energy required to bend a right triangle is given by:

$$U^{2D}_{crease} = -\frac{1}{6} f_a \frac{m^2 l^2}{n} + C\sqrt{k f_a n m l} \tag{3.50}$$

where $C = \frac{4}{3}\left(2 - \sqrt{2}\right)$, f_a is the downward force per area, k is the bending modulus, m is the width of the sheet (minus the fixed length), l is the crack length, and $n = \sqrt{m^2 + l^2}$.

For initial cracks that are much smaller than the width of the sheet, that is $l << m$:

$$U^{2D}_{l<<m} = -\frac{1}{6} f_a m l^2 + C m \sqrt{k f_a l} \tag{3.51}$$

3.5.4 Griffith Point

In Sec. 3.2 we presented the Griffith's criterion for a crack to propagate on a 2D sheet, Eq. (3.3):

$$\frac{dU_{out}}{dl} + \Gamma = 0$$

Substituting the energy outside the crack tip, U_{out}, for the energy to bend a triangle, Eq. (3.50), and solving for the minimum force for the crack to run, we obtain our **final expression for an edge crack**:

$$\begin{aligned} f_a^{edge} = \frac{3(l^2+m^2)^{3/2}}{2l^3m^3(l^2+2m^2)^2}\Big[&3C^2k(2l^2+m^2)^2 + 4\Gamma l^2 m(l^2+2m^2) \\ &+ C(2l^2+m^2)\sqrt{3k(3C^2k(2l^2+m^2)^2 + 8\Gamma l^2 m(l^2+2m^2))}\Big] \end{aligned} \tag{3.52}$$

where l is the crack length, m is the width of the sheet (minus the fixed length), k is the bending modulus Eq. (3.15), Γ is the surface energy density Eq. (3.16), and $C = \frac{4}{3}\left(2 - \sqrt{2}\right)$. See Fig. 3.22.

For a crack in the middle of the sheet, as there are two folds, the total energy outside the crack tip is:

$$U_{out} = 2U^{2D}_{crease} \tag{3.53}$$

Hence our **final expression for a crack in the middle of the sheet** is:

$$f_a^{middle} = \frac{3(l^2+\tilde{m}^2)^{3/2}}{2l^3\tilde{m}^3(l^2+2\tilde{m}^2)^2}\Big[3C^2k(2l^2+\tilde{m}^2)^2 + 2\Gamma l^2\tilde{m}(l^2+2\tilde{m}^2) \\ +C(2l^2+\tilde{m}^2)\sqrt{3k(3C^2k(2l^2+\tilde{m}^2)^2+4\Gamma l^2\tilde{m}(l^2+2\tilde{m}^2))}\Big] \tag{3.54}$$

where $\tilde{m}$ is **half** of the width of the sheet (minus the fixed length) for a sheet with crack in the middle.

Following the same procedure for initial cracks that are much smaller than the width of the sheet ($l << m$), Eq. (3.51), we find:

$$f_a^{edge_{l<<m}} = 3\frac{\Gamma}{ml} + \frac{3C}{8l^3}\left[3Ck + \sqrt{3k\left(3C^2k + 16\Gamma\frac{l^2}{m}\right)}\right] \tag{3.55}$$

and:

$$f_a^{middle_{l<<\tilde{m}}} = \frac{3}{2}\frac{\Gamma}{\tilde{m}l} + \frac{3C}{8l^3}\left[3Ck + \sqrt{3k\left(3C^2k + 8\Gamma\frac{l^2}{\tilde{m}}\right)}\right] \tag{3.56}$$

Note that these expressions for the minimum force required for a crack to run, depend not only on the crack length, l, like the previous results, Eq. (3.13) and (3.21), but also on the width of the sheet, m, (or the half-width, $\tilde{m}$). Fig. 3.24 shows two graphs of force versus initial crack length for a sheet with a crack in the middle. The half width of the sheet, $\tilde{m}$, in Fig. 3.24b

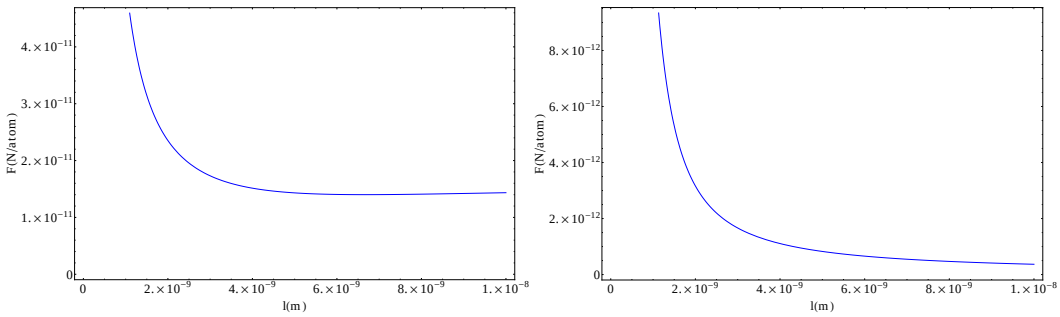

(a) $\tilde{m} = 50 \times 10^{-10}$meters (b) $\tilde{m} = 500 \times 10^{-10}$meters

Figure 3.24: Plot of force (in Newtons per atom) versus initial crack length (in meters), Eq. (3.54). The half width of the sheet, $\tilde{m}$, in Fig. 3.24b is 10 times larger than the one in Fig. 3.24a.

is 10 times larger than the one in Fig. 3.24a. Notice that longer initial crack lengths lead to lower minimum forces. Also, wider sheets lead to lower minimum forces. As a result, the minimum force approaches zero with increasing initial crack length **and** width of the sheets.

3.5.5 Numerical study of improved theory

Here we present a comparison of the numerical results of sheets with a crack at the edge and with a crack in the middle, Secs. 3.3.2 and 3.4.2.2, with the new analytical expressions obtained in the previous section. We use the values of the bending modulus k, Eq. (3.15), and of the surface energy density Γ, Eq. (3.16), for graphene discussed previously (Sec. 3.3.2).

3.5.5.1 Numerical study of a sheet with a crack in the middle

A graph of force per atom versus initial crack length for a wide-open crack in the middle of the sheet is shown in Fig. 3.25. The line is the theoretical expression, Eq. (3.54), the dashed line is the approximation for initial cracks that are much smaller than the width of the sheet, $l << m$, Eq. (3.56), and the dots are the numerical results. Again the horizontal error bars are estimated uncertainties of the initial crack length due to the fact that the crack tip is not well defined. The vertical error bars are due to the precision of our numerical simulations.

The graph shows a much better agreement between the theory and the simulations than before, but longer initial crack lengths lead to clear differences between the two. All the simulations shown so far were for sheets of 100Å by 100Å. As the theory is scalable, we used small samples to save computational time. Numerically, long initial crack lengths can suffer from edge effects. To test if our issues are due to edge effects we applied the same initial crack lengths on a sheet of 200Å by 100Å, that is, we kept the same width, m, and changed only the sheet's length, a parameter that the theory is independent of. The result is shown in Fig. 3.26 and 3.27. The line is the theoretical expression, Eq. (3.54), the dots are the numerical results for a sheet of 100Å $\times$ 100Å, and the triangles are the numerical results for a sheet of 200Å $\times$ 100Å. Notice how for short initial cracks both results fall exactly on top of each other. Now for long initial cracks the force basically plateaus for the 200Å $\times$ 100Å sheet, similar to the theory, while for the 100Å $\times$ 100Å sheet the force continues to

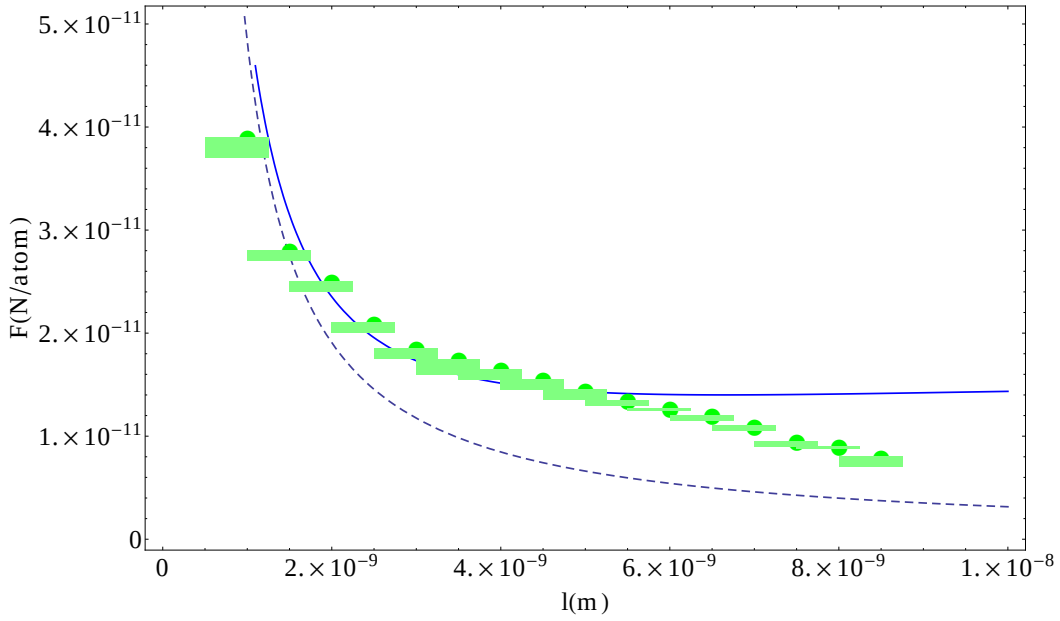

Figure 3.25: Graph of force (in Newtons per atom) vs initial crack length (in meters) for a wide-open middle crack. The line is the theoretical expression, Eq. (3.54), the dashed line is the approximation $l << m$, Eq. (3.56), and the numerical results are the the dots with the error bars.

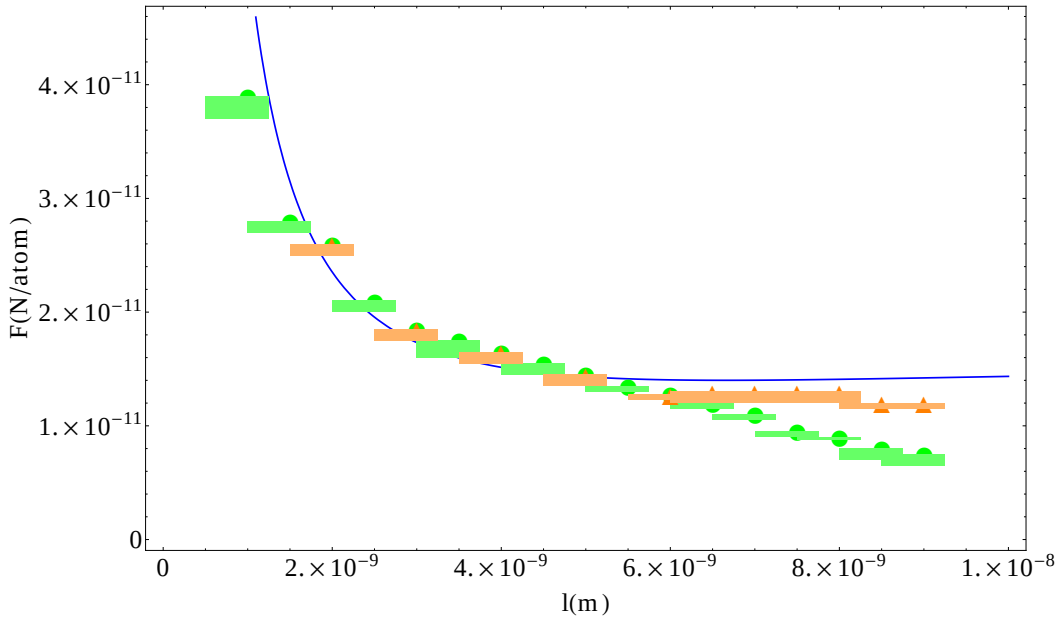

Figure 3.26: Graph of force (in Newtons per atom) vs initial crack length (in meters) for a wide-open middle crack. The line is the theoretical expression, Eq. (3.54), the green dots are the numerical results for a sheet of 100Å × 100Å, and the orange triangles are the numerical results for a sheet of 200Å × 100Å.

decrease, due to edge effects.

Another issue is that it is hard to produce short initial cracks in the middle of the sheet. They close easily and the uncertainty of the crack tip plays an important role. Therefore, the uncertainties for the first two points on the graphs (initial cracks of 10Å and 15Å) are probably higher than the values presented on Fig. 3.25.

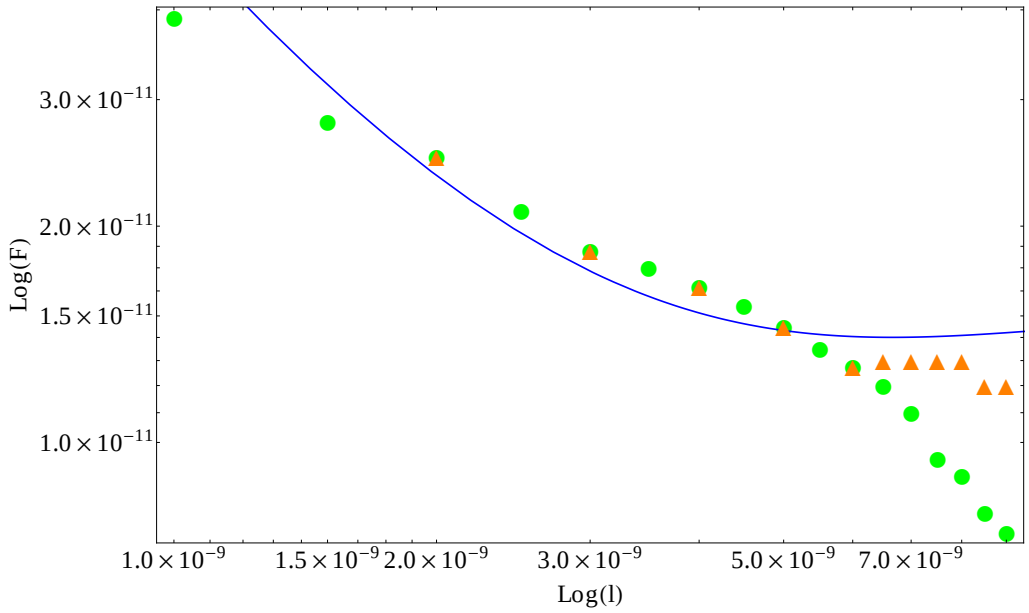

Figure 3.27: Log-log graph of force (in Newtons per atom) vs initial crack length (in meters) for a wide-open middle crack. The line is the theoretical expression, Eq. (3.54), the dots are the numerical results for a sheet of 100Å × 100Å, and the triangles are the numerical results for a sheet of 200Å × 100Å.

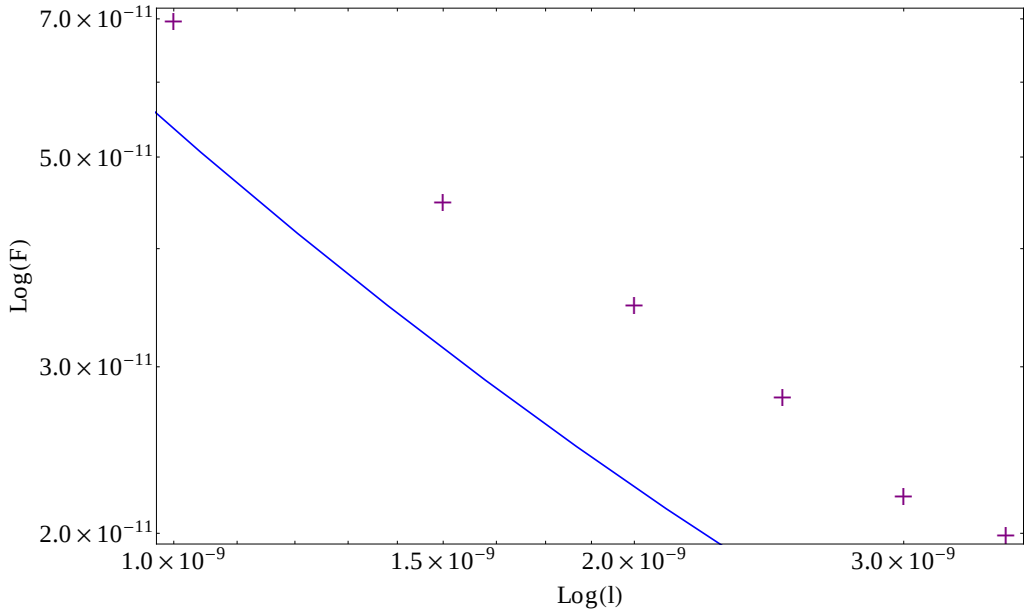

Figure 3.28: Log-log graph of force (in Newtons per atom) vs initial crack length (in meters) for an edge crack. The line is the theoretical expression, Eq. 3.52, and the plus symbols are the numerical results.

3.5.5.2 Numerical study of sheet with an edge crack

Now let us consider the case of an edge crack. Fig. 3.28 shows a log-log graph of force per atom versus initial crack length. The line is the theoretical expression, Eq. (3.52), and the plus symbols are the numerical results. In this case the numerical results and the theory follow the same trend, but they do not seem to agree as well.

Looking at the simulations of sheets with an initial edge crack we notice that the crease seems to end before the fixed end, see Fig. 3.29. This means that the value for m should be smaller than the width of the sheet minus the

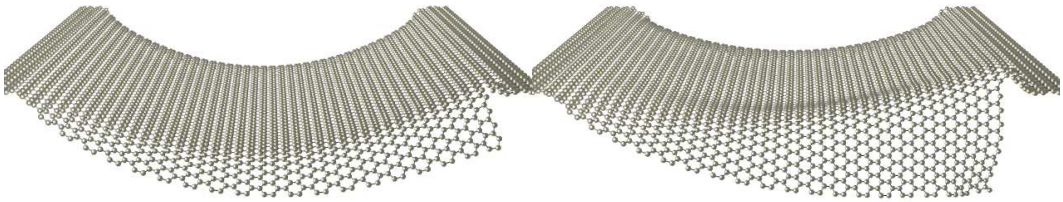

(a) initial edge crack of $l \approx 10$Å (b) initial edge crack of $l \approx 25$Å

Figure 3.29: Clamped, free-standing graphene sheets with an initial edge crack under a downward constant force. The sheets exhibits a crease before the crack runs. The crease starts at the crack tip and ends before the fixed end.

width of both fixed ends. The best fit for the theoretical expression Eq. (3.52) with the numerical results, assuming m to be a fitting parameter, is shown in Fig. 3.30. The width of the sheet minus the fixed ends is ≈ 90Å and best fit value for m is 64Å. At this point, it is hard to determine the crease length from the simulations and further studies of a sheet with an initial edge crack need to be pursued, as our preliminary results constitute of only a few data points.

These simple analytical expressions for the minimum force required for a crack to run, Eq. (3.52) and Eq. (3.54), offer insight into the tearing of graphene, and suggest the order of magnitude for the forces to be used or avoided in experiments. Also, experiments can obtain the value for the tearing energy density Γ of graphene (a quantity we have not been able to find in the literature) by combining our theory with measurements of initial crack length and applied force.

In the near future we want to extend our numerical study to crack

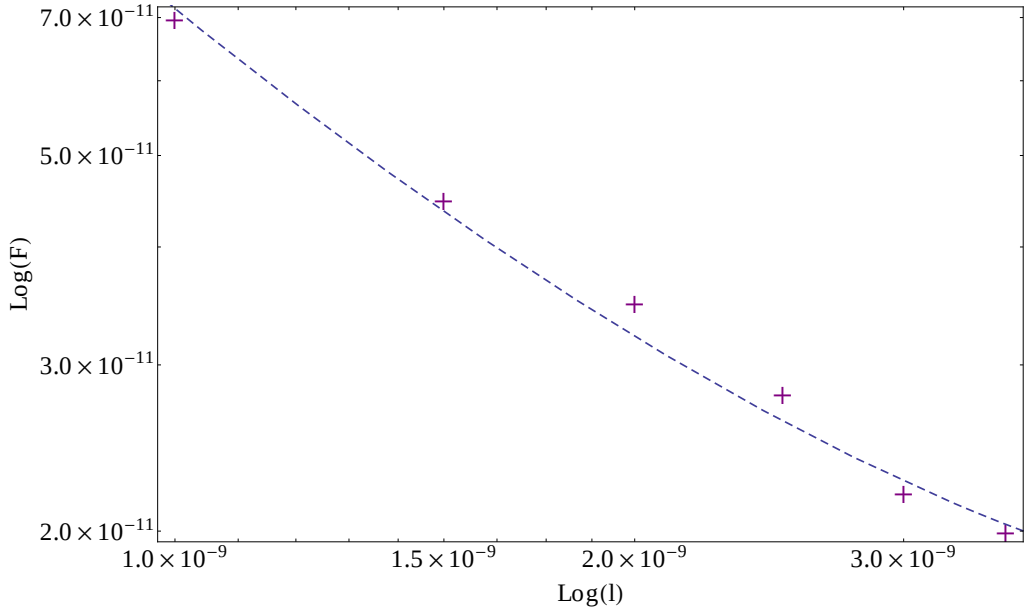

Figure 3.30: Log-log graph of force (in Newtons per atom) vs initial crack length (in meters) for an edge crack. The dashed line is the best fit for theoretical expression, Eq. (3.52), assuming m to be a fitting parameter, and the plus symbols are the numerical results. The width of the sheet minus the fixed ends is 90Å and the best fit value for m is 64Å.

propagation in different types of edges, zigzag versus armchair. We also would like to look at the effects of impurities to the crack propagation dynamics.

3.6 Experiments

The fracture of free-standing graphene sheets is in general an undesirable occurrence. Most experiments do not report or take measurements of such events. As a consequence it has been hard to gather experimental data on this problem.

We learned about this problem from a conversation Prof. MacDonald had with Prof. Bolotin from Vanderbilt University. Prof. Bolotin has observed the fracture of free-standing graphene in multiple experimental setups, including the back-gate voltage. His samples exhibit cracks at the edge and in the middle, Fig. 3.31, 3.32, and 3.33. The graphene samples used in his experiments are obtained either by the micromechanical cleavage method [53] or grown by chemical vapor deposition (CVD) [36]. The experimental samples are about 2 by 2μm, and stand about $z_{substrate} = 150$nm from the substrate. In the back-gate voltage setup they use voltages of V=2-3V. Based on this information we can estimate the force that a free-standing graphene sheet is subjected to in the back-gate voltage setup. The electric field that acts on the graphene sheet is given by:

$$E = \frac{V}{z_{substrate}} \approx 20 \times 10^6 \text{V/m} \tag{3.57}$$

The force per area exerted on the graphene sheet is then:

$$f_a^{exp} = E^2 \cdot \epsilon_0 \approx 3541\text{N/m}^2 \tag{3.58}$$

Numerically we use force per atom, Eq. (3.18), hence:

$$f_{atom}^{exp} = \frac{f_a^{exp}}{38.17 \times 10^{18}\text{m}^{-2}} \approx 1 \times 10^{-16}\text{N/atom} \tag{3.59}$$

Having the force, Eq.(3.59), and the width of the samples we can obtain the initial crack length, Eq. (3.54) (or Eq. (3.52)):

$$l_{middle} \approx l_{edge} \approx 1.5 \times 10^{-6}\text{m} \tag{3.60}$$

This is a large value considering that the samples are 2 by 2μm, but keep in mind this is just an estimate.

On the other hand, we can look at the problem from the crack length point of view. Considering a more reasonable crack length, for example, a crack of about 10% of the sheet's length, $l \approx 0.2 \times 10^{-6}$m. From Eq. (3.54) (or Eq. (3.52)) we obtain that the minimum force required for the crack to run is:

$$f^{10\%crack} \approx 8 \times 10^{-16}\text{N/atom}, \tag{3.61}$$

which is of the same order of magnitude as Eq. (3.59).

A problem with the values for the initial crack length, Eq. (3.60), and the force, Eq. (3.61), is that to find those we need the surface energy density Γ. Because we have not been able to find an experimental value for this quantity in the literature we used the value we obtained numerically, Eq. 3.16. However,

according to the theory of fracture mechanics, this parameter needs to come from experimental measurements.

A graph of force per atom versus initial crack length, considering the width of the crease to be $m = 2\mu$m (therefore $\tilde{m} = 1\mu$m) is shown in Fig. 3.34. The line is the theoretical expression for a crack in the middle of the sheet, Eq. (3.54), and the dashed line is the expression for a crack at the edge, Eq. (3.52). Note that, for initial cracks smaller than the sheet's width, the minimum force required for a crack to run is very similar for a crack at the edge and for a crack in the middle of the sheet.

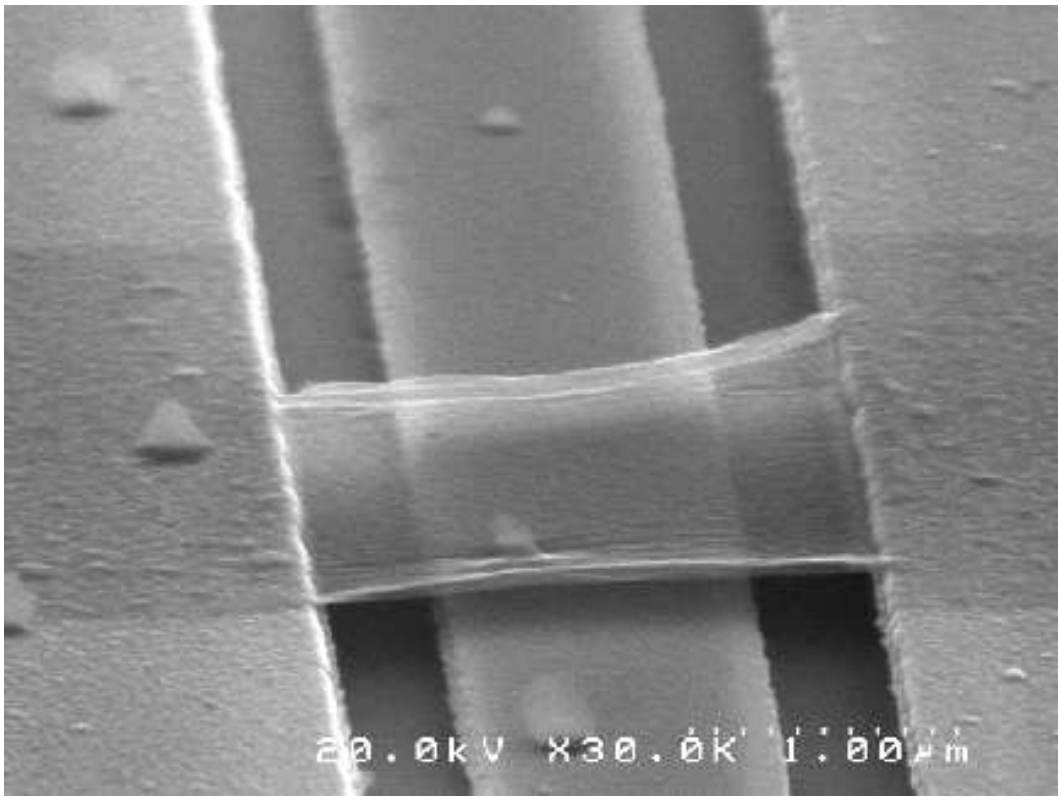

Figure 3.31: Image courtesy of Hiram Conley, Bolotin Research Group: Fracture in CVD graphene. Note the crease going from the crack on the left side all the way to the fixed edge on the right.

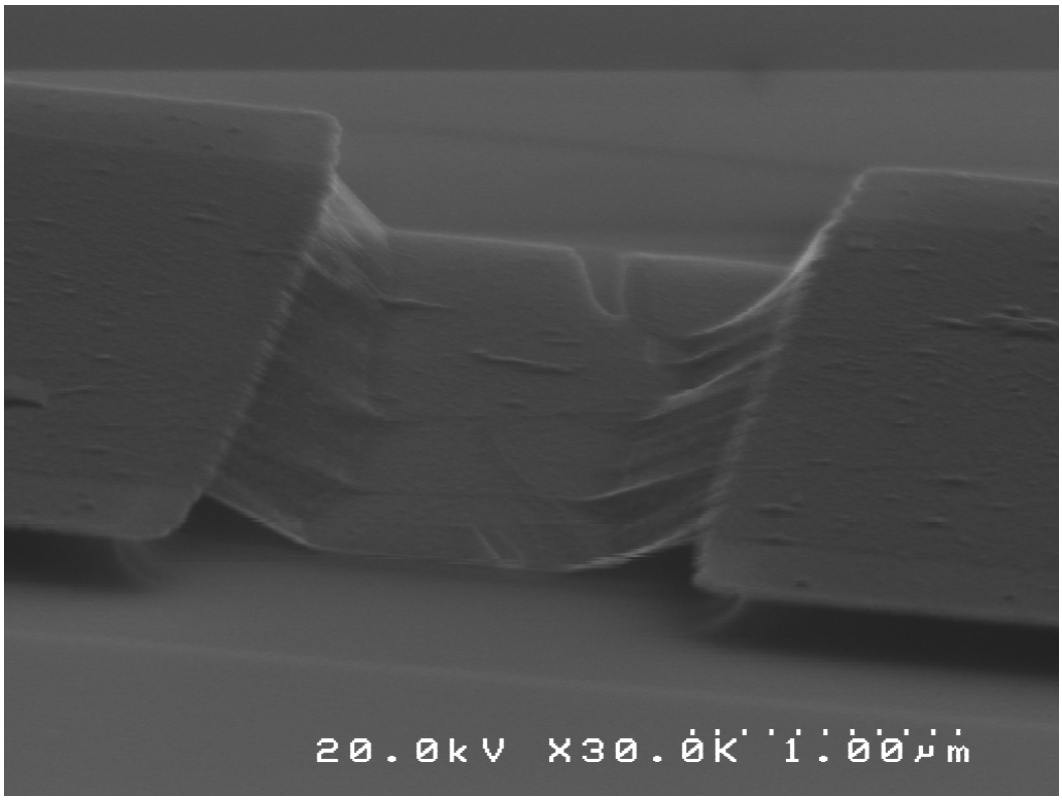

Figure 3.32: Image courtesy of Hiram Conley, Bolotin Research Group: Fracture in CVD graphene.

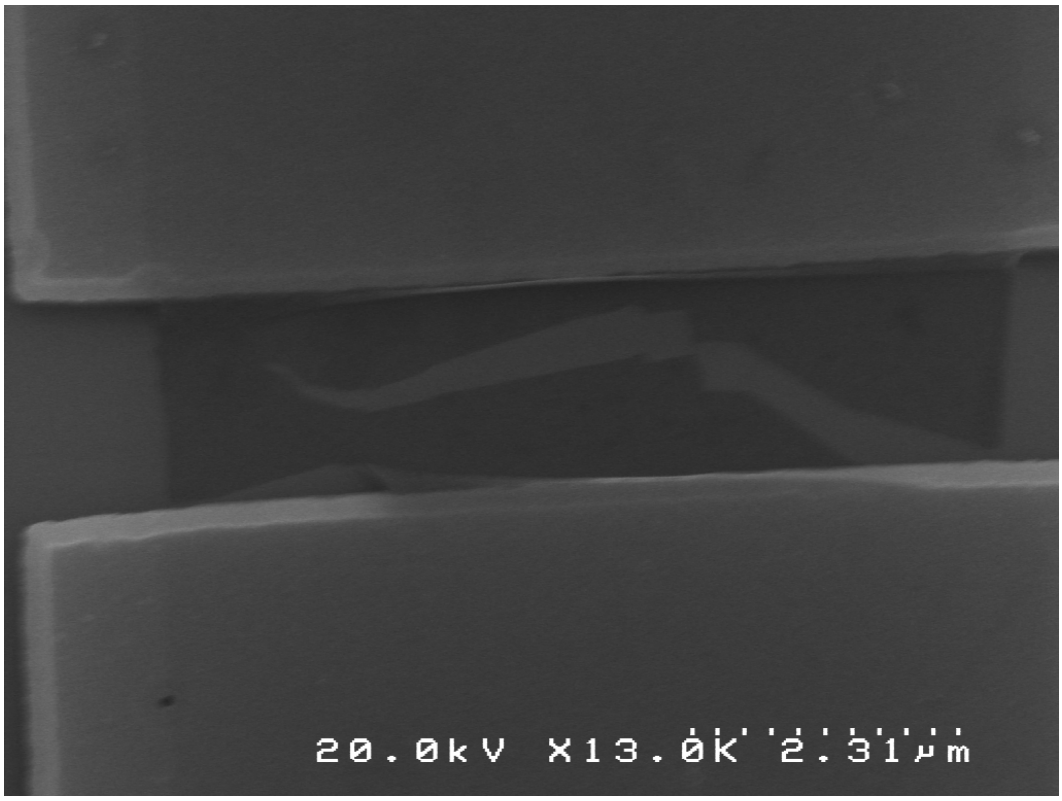

Figure 3.33: Image courtesy of Hiram Conley, Bolotin Research Group: Top view of fracture in CVD graphene.

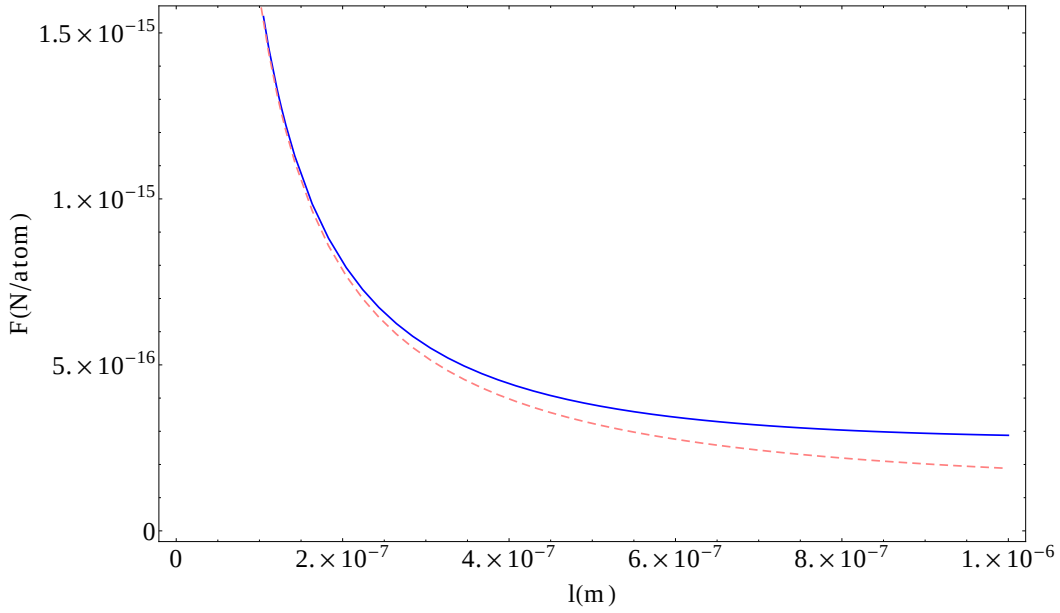

Figure 3.34: Graph of force (in Newtons per atom) vs initial crack length (in meters). The line is the theoretical expression for a crack in the middle of the sheet, Eq. (3.54), with $\tilde{m} = 1\mu$m. The dashed line is for a crack at the edge, Eq. (3.56), with $m = 2\mu$m.

Chapter 4

Results and conclusions

In this work we presented numerical simulations and analytical calculations for ripples and cracks in graphene. The problems addressed were motivated by experimental observations. Below are our results and conclusions for each of the topics.

4.1 Ripples in graphene

Meyer *et al.* observed that free-standing graphene sheets exhibit crumpling [45]. The ripples observed in experiments are estimated to be 2 to 20Å high and 20 to 200Å wide.

In Chap. 2 we showed that the crumpling is not due to thermal fluctuations, as previously proposed [8, 19]. Thermally excited ripples oscillate at frequencies too high to be resolved by diffraction experiments (10^9-10^{11}Hz). Therefore they should produce sharp Bragg peaks, which disagrees with the experimental observations of broad peaks [45].

We also showed that the Mermin-Wagner theorem [43] is irrelevant for free-standing graphene, as the length scale for a graphene sheet to lose translational order at room temperature is much larger than experimental

graphene sample sizes.

We presented numerical studies of free-standing graphene, both with and without surface impurities. The simulations use the MEAM semi-empirical potential [9] and damped molecular dynamics. In an effort to better model the experimental conditions, all the simulations in this work are of finite-sized graphene sheets, in contrast to previous works [8, 19] that rely on periodic boundary conditions. These simulations were done at zero temperature, to focus on effects not due to temperature.

We observe that finite-sized graphene exhibits edge effects because of under-coordinated edge atoms, Fig. 4.1a. The ripples due to edge effects are $\approx$30Å wide and $\approx$10Å high. They occur, however, only at the edge of the system, and the amplitude decays to zero on the scale of 3.2Å. Thus, edge effects alone cannot explain the ripples observed in experiments.

We proposed that graphene sheets ripple as a consequence of the adsorption of impurities at random sites throughout the crystal. It is common for graphene samples to be exposed to the environment and thereby adsorb impurities such as water, OH, H, etc. [17, 24, 47].

Our simulations reveal that impurities on the surface of graphene sheets cause them to ripple, Fig. 4.1b. The amplitude of the ripples increases with the concentration of impurities, while the wavelength stays almost constant, Fig. 4.2.

A graphene sheet with a 5 to 20% concentration of OH develops rip-

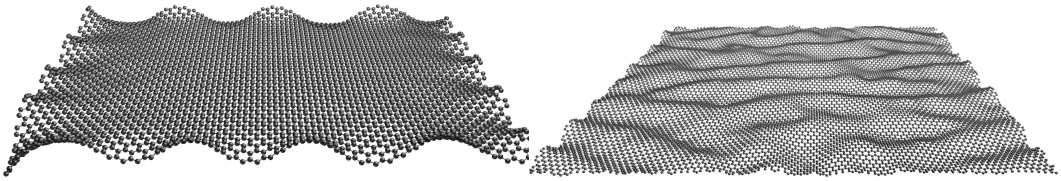

(a) Ripples caused by edge effects (b) Ripples caused by impurities

Figure 4.1: Fig. 4.1a Ripples in graphene produced by edge effects alone in graphene sheet of 100Å × 100Å. Fig. 4.1b Ripples in graphene produced by 20% coverage of OH, 200Å × 200Å system.

ples whose wavelength and amplitude are comparable to those seen in experiment. Experimentalists say that 20% concentration of impurities is unlikely to happen on pristine graphene [1, 6]. These would be more likely in graphane (graphene+CH_2) and graphene oxide.

We should also note that our results show that the MEAM potential overstates the bending energy of graphene, so it will tend to underestimate the scale of ripples.

Experiments that use processes to reduce impurities on graphene sheets, such as annealing, observe a reduction of the rippling of the sheets [26], in agreement with our simulations.

After the publication of this work questions were posed [6] that challenge the parameter range on which our numerical work focused. It was brought to our attention [6] that high concentrations of OH radicals would change the transport electronic properties of pristine graphene, as the OH radical will react with the defect-free basal plane of graphene, changing the bonding (as described in our work) and therefore creating a chemical function-

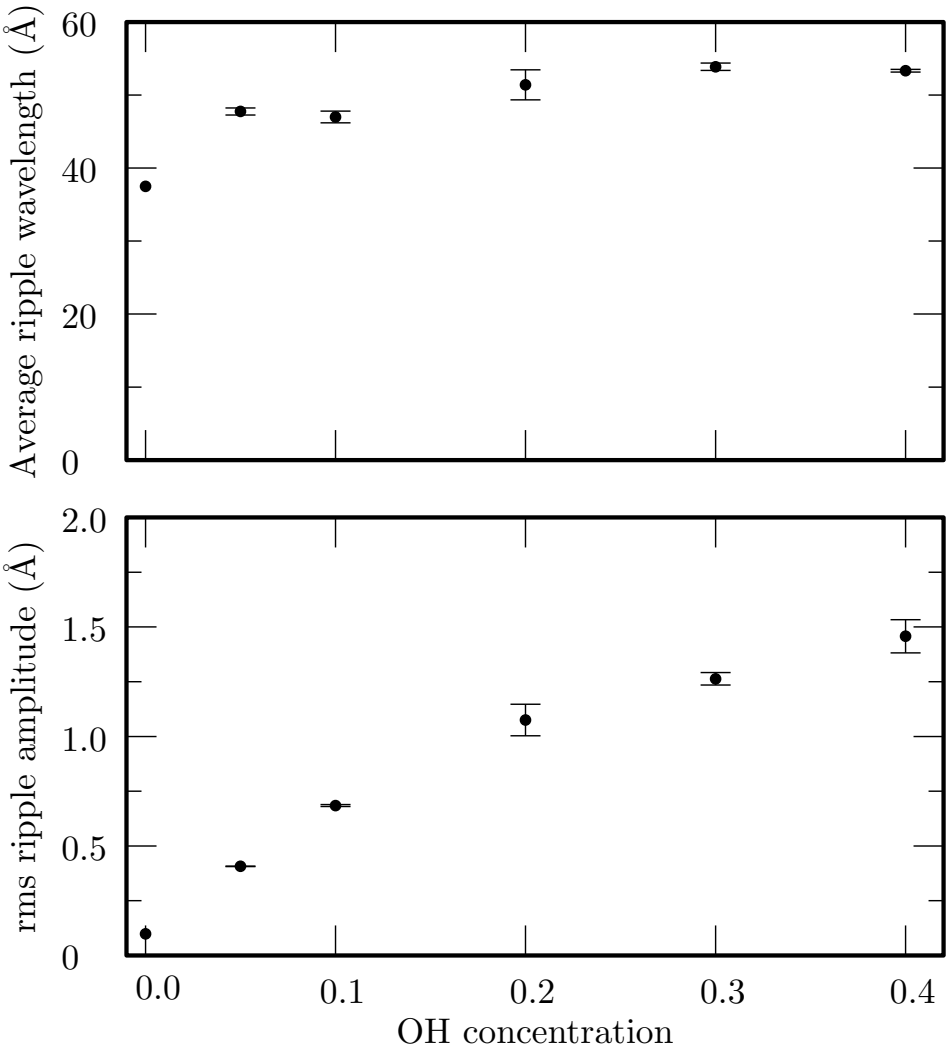

Figure 4.2: Wavelength and amplitude of buckles versus OH concentration in 200Å $\times$ 200Å sheets. Amplitudes of the rippled peaks are around six times larger than the rms amplitude. Wavelength and rms amplitude were computed after excluding 20Å of material at the edge of the sample. Wavelength was computed by decomposing the sheet into a series of line scans, taking the one-dimensional Fourier transform of them in turn, finding the average wave vector $\bar{k}$ for each line weighted by the amplitude of the Fourier transform, computing $\lambda = 2\pi/\bar{k}$ and finally averaging λ over all the line scans. Error bars represent standard errors after averaging over three independent trials per concentration.

alization of graphene in which each C having a covalently attached hydroxyl group, i.e., -C-OH, will be in the sp^3 bonding state. Such changes in electronic properties are not observed in experiments, which strongly suggests that OH radicals play little role. Nevertheless, the fact that graphene ripples means that changes in at least some bond lengths is a geometrical necessity. We can see two possible resolutions of this problem that should be examined in the future:

1. Figure 4.2 shows that the ripple amplitude is largely unchanged down to the smallest concentrations of distorted bonds we studied. An examination of the concentration range below 5% might find ripple wavelengths and amplitudes that are still compatible with experiment, but involve experimentally plausible concentrations of free radicals.

2. Non-reactive adsorbates, such as water, ethanol, and various hydrocarbons, are known to be present on graphene at much higher concentrations than covalently attached groups arising, e.g., from reaction with free radicals. These could affect equilibrium bond lengths much less. Perhaps a high concentration of much weaker bond distortions could create similar ripples. Checking this point will require further study.

There are two important points to keep in mind. First, it is still hard to determine the concentration of adsorbates, both computationally and experimentally. And second, in this work we focus on one effect that does create ripples in graphene (namely, changing C-C bond lengths "within the sheet"),

while we acknowledge that there are other contributions in the experimental environment, such as defects and impurities in/on the graphene sheet, it interacts with microscope tips (STM, AFM, ...), it is possibly heated by interrogating probes such as the electrons incident from TEM, the sheets are suspended with particular boundary conditions in different configurations, and so on.

4.2 Cracks in graphene

In some experimental setups free-standing graphene samples show cracks and holes, and sometimes the samples even break [2, 3, 5, 30, 67]. In Chap. 3 we showed that out-of-plane forces can cause free-standing graphene to fracture. This fracture mode is known as the tearing mode and is common in materials such as paper.

4.2.1 Numerical studies

We presented a numerical study of the propagation of cracks in clamped, free-standing graphene as a function of the out-of-plane force. The simulation uses the MEAM semi-empirical potential [9] and damped molecular dynamics. Again no periodic boundary conditions were used, to better model the experimental conditions.

Most experiments focus on electronic properties, and do not look at initial cracks in the samples. Consequently, the shapes of the cracks are in general unknown. We considered two possible initial conditions: a crack at the very edge of the sheet and a crack in the middle of the sheet. As an example

of an initial condition, Fig. 4.3a shows an initial crack of 15Å in the middle of a suspended graphene sheet. Once sufficient downward force is applied on the sheet the crack starts running, as seen on Fig. 4.3c. We have also made videos of crack propagations. Appendix D has a link to some movies.

The simulations show that cracks in the middle of the sheet always run straight, while cracks at the edge do not (see Fig. 4.3c and 4.4b). The propagation pattern of an edge crack is dependent on the initial condition. Fig. 4.4b shows an initial zigzag crack propagating as armchair and then as zigzag again. Similar dynamics have been seen in simulations of tearing graphene nanoribbons [27, 30].

Another interesting numerical result is that the sheet folds in a crease before the crack runs, both for sheets with a cracks in the middle (on both sides of the crack) and at the edge, Fig. 4.4a. In experiments, folds, scrolls, and creases are commonly observed in free-standing graphene samples.

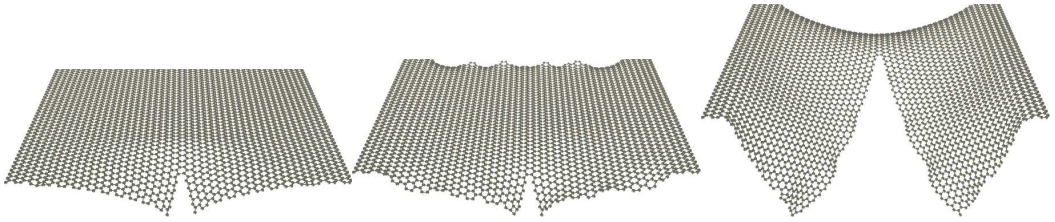

(a) initial crack of $l \approx 15$Å (b) sheet wrinkles and bends (c) crack propagates

Figure 4.3: Constant downward force is applied on a 100Å by 100Å clamped, free-standing graphene sheet with an initial crack of $l \approx 15$Å. Notice that the sheet wrinkles and bends before the crack runs.

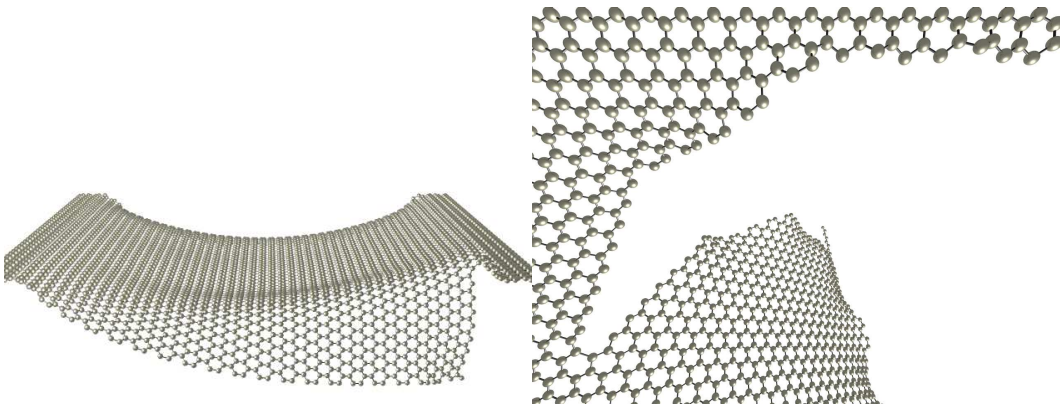

(a) initial edge crack of $l \approx 25$Å (b) initial edge crack of $l \approx 30$Å

Figure 4.4: Clamped, free-standing graphene sheets with an initial edge crack under a constant downward force. Fig 4.4a: The sheets exhibits a crease just before the crack runs. Fig. 4.4b: Non-straight crack propagation - the initial zigzag crack propagates as armchair and then turns zigzag again.

4.2.2 Analytical studies

We presented an analytical study of the tearing of a two dimensional sheet, such as graphene, and obtained as a function of the initial crack length the minimum force required for a crack to run.

We started by considering a sheet with an initial crack of length l. The crack can run a length dl if doing so reduces the total energy of the system. From that we obtained the Griffith's criterion for a crack to propagate in a two-dimensional sheet:

$$\frac{dU_{out}}{dl} + \Gamma < 0, \tag{4.1}$$

where Γ is the surface energy of graphene, which can be measured experimentally, and U_{out} is the energy outside the crack tip, which depends on the

geometry of the system.

In the case of a sheet with an initial crack of length l (at the edge or in the middle of the sheet) the energy outside the crack tip U_{out} is equivalent to the energy required to bend a two-dimensional sheet.

In our first analytical study we assumed the small bending approximation, Eq. (3.8). Because the numerical simulations show that the sheets folds in a crease, Fig. 4.4a, this approximation is not appropriate for suspended graphene.

We then presented a theory for a sheet folding in a crease. We considered the crease to go from the crack tip all the way to the fixed end, forming a right triangle as shown in Fig. 4.5. The triangle has one side of length l, the crack length, and another side of length m, the width of the sheet (minus the fixed length, assuming the sheet bends all the way to the fixed end).

We found that the minimum downward force (per area) required for a crack to run on a clamped, free-standing sheet is

1. for an edge crack:

$$f_a^{edge} = \frac{3(l^2+m^2)^{3/2}}{2l^3m^3(l^2+2m^2)^2}\Big[3C^2k(2l^2+m^2)^2 + 4\Gamma l^2 m(l^2+2m^2) \\ +C(2l^2+m^2)\sqrt{3k(3C^2k(2l^2+m^2)^2+8\Gamma l^2 m(l^2+2m^2))}\Big] \quad (4.2)$$

2. for a crack in the middle of the sheet:

$$f_a^{middle} = \frac{3(l^2+\tilde{m}^2)^{3/2}}{2l^3\tilde{m}^3(l^2+2\tilde{m}^2)^2}\Big[3C^2k(2l^2+\tilde{m}^2)^2 + 2\Gamma l^2 \tilde{m}(l^2+2\tilde{m}^2) \\ +C(2l^2+\tilde{m}^2)\sqrt{3k(3C^2k(2l^2+\tilde{m}^2)^2+4\Gamma l^2 \tilde{m}(l^2+2\tilde{m}^2))}\Big], \quad (4.3)$$

where l is the crack length, k is the bending modulus, Eq. (3.15), Γ is the surface energy density, Eq. (3.16), $C = \frac{4}{3}\left(2-\sqrt{2}\right)$, m is the width of the sheet (minus the fixed length), and $\tilde{m}$ is **half** of the width of the sheet (minus the fixed length) for a sheet with crack in the middle. See Fig. 4.5.

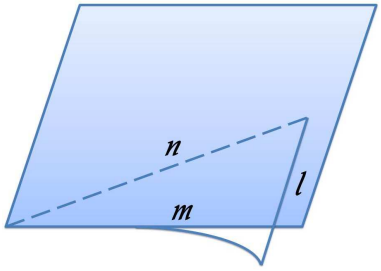

Figure 4.5: Suspended sheet with an initial crack of length l. The triangle formed by the crease is the part of the sheet that is initially free to bend, because it is not attached to the support.

These expressions show that longer initial crack lengths lead to lower minimum forces, Fig. 4.6. Also, wider sheets lead to lower minimum forces. As a result, the minimum force approaches zero with increasing initial crack length **and** width of the sheets.

Another interesting result is that, for initial cracks smaller than the sheet's width, the minimum force required for a crack to run is very similar for a crack at the edge and for a crack in the middle of the sheet, Fig. 3.34.

4.2.3 Conclusions

The numerical fracture forces show good agreement with the analytical fracture forces for cracks in the middle of the sheet, Fig. 4.6. For cracks at the

edge the numerical results and the theory follow the same trend, but they do not seem to agree as well. This might be because for edge cracks the crease seems to end before the fixed end, Fig. 4.4a. At this point, it is difficult to determine the crease length from the simulations. Further studies of a sheet with an initial edge crack need to be pursued, because our preliminary results constitute of only a few data points.

It has been difficult to gather experimental data on this problem, because the fracture of free-standing graphene sheets is in general a an undesirable occurrence. Therefore most experiments do not report or take measurements of such events. Preliminary results show that, for initial crack lengths of about 10% of the graphene sample's length, our expression for the minimum force required for a crack to run, Eq. (4.2) and (4.3), results in forces comparable to the forces a free-standing graphene is subjected to in a back-gate voltage experiment.

The analytical expressions for the the minimum force required to tear a two dimensional sheet, such as graphene, in terms of the initial crack length, offer insight into the tearing of graphene, and suggest the order of magnitude for the forces to be used or avoided in experiments. Also, experiments can obtain the value for the tearing surface energy density of graphene (a quantity we have not been able to find in the literature) by combining our theory with measurements of initial crack length and applied force.

In the near future we want to extend our numerical study to investigate crack propagation in zigzag edges and armchair edges. We also would like to

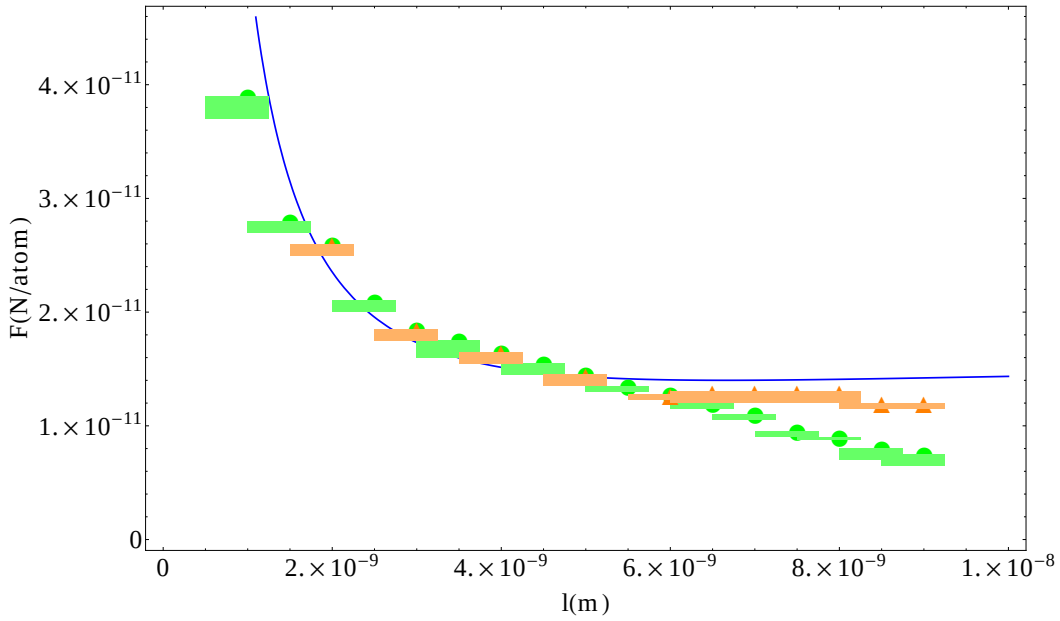

Figure 4.6: Graph of force (in Newtons per atom) vs initial crack length (in meters) for a wide-open middle crack. The line is the theoretical expression, Eq. (3.54), the green dots are the numerical results for a sheet of 100Å × 100Å, and the orange triangles are the numerical results for a sheet of 200Å × 100Å. Note that long cracks on the 100Å × 100Å sheet are influenced by edge effects.

look at the effects of impurities on the crack propagation dynamics.

Appendices

Appendix A

About the code

The code used in this work was initially written by Dominic Holland in the late 1990's. Since then it has been used by many of Prof. Marder's students and has grown considerably. Holland makes a great statement about the code in his thesis: "the tool itself, sophisticated software running on large supercomputers, can be quiet an absorbing and seductive thing, requiring a great deal of effort to develop, even to the point of distraction from the supposed target physics, and somewhere along the line becoming a satisfying end in itself". The code is a powerful tool, but it is very complex and I spent most of my PhD studies learning and troubleshooting it. It is a picky code, it is not easy to run it in any machine and it requires specific configurations and versions of programs. I have not run it in supercomputers or used it for parallel computing.

The code is written in C and wrapped around by Python. My current version of the code has are approximately 150 subroutines. The routines deal with multiple potentials, strain, fracture modes, phase transformations and patterns in granular media, and more. The code can work with amorphous, vitreous or crystalline solids, liquids or gases, or collections of grains.

I only used it to study rippling and fracture of free-standing graphene. I also contributed to it with routines related to initial conditions and fracture.

The following is a brief explanation of how the code works. We start with the setup files, where we choose types of atoms, initial conditions, potential to be used, size and number of time steps, boundary conditions, if there will be strain, fracture, etc. These files also provide the parameters of the potentials. Then we move to making the crystal. According to the choice of atoms, type of crystal, sample size, and possible defects the code uses the provided primitive vectors and constrains to build the initial crystal lattice. Then the energy (potential and kinetic) is calculated according to the chosen potential. The energy is minimized using damped molecular dynamics, more specifically verlet. Many output files are constantly generated, containing the initial crystal configurations, the position and velocity of each atom, and the energy (potential and kinetic) of the system. Finally beautiful graphics are made using POV-Ray (a free tool for creating three-dimensional graphics).

Appendix B

Modified Embedded Atom Method (MEAM)

The Modified Embedded Atom Method (MEAM) is a semi-empirical interatomic potential, based on density functional theory (it considers the superimposition of atomic density). It has been tested for many materials [9, 10, 25], including single layer graphene [35].

The main idea of the Modified Embedded Atom Method is to describe the energy it takes to embed an atom in the background electron density. In MEAM, the total energy of the system is approximated as:

$$E = \sum_i \left[F_i(\bar{\rho}_i) + \frac{1}{2} \sum_{j \neq i} S_{ij} \phi_{ij}(R_{ij}) \right] \tag{B.1}$$

where F_i is the embedding function, $\bar{\rho}_i$ is the background electron density at site i, S_{ij} and $\phi_{ij}(R_{ij})$ are the screening factor and the pair interaction between atom i and j separated by a distance R_{ij}.

To find $\bar{\rho}$ a weighted sum of partial background densities is found:

$$(\bar{\rho}_i)^2 = \sum_{l=0}^{3} t_i^{(l)} \left(\rho_i^{(l)} \right)^2 \tag{B.2}$$

where t_i is a material dependent parameter. There are four terms in the sum that follow the symmetry of the s, p, d and f orbitals:

$$\rho_i^{(0)} = \sum_{j \neq i} \rho_j^{a(0)}(R_{ij}) \tag{B.3}$$

$$\left(\rho_i^{(1)}\right)^2 = \sum_{\alpha} \left[\sum_{j \neq i} x_{ij}^{\alpha} \rho_j^{a(1)}(R_{ij})\right]^2 \tag{B.4}$$

$$\left(\rho_i^{(2)}\right)^2 = \sum_{\alpha,\beta} \left[\sum_{j \neq i} x_{ij}^{\alpha} x_{ij}^{\beta} \rho_j^{a(2)}(R_{ij})\right]^2 - \frac{1}{3}\left[\sum_{j \neq i} \rho_j^{a(2)}(R_{ij})\right]^2 \tag{B.5}$$

$$\left(\rho_i^{(3)}\right)^2 = \sum_{\alpha,\beta,\gamma} \left[\sum_{j \neq i} x_{ij}^{\alpha} x_{ij}^{\beta} x_{ij}^{\gamma} \rho_j^{a(3)}(R_{ij})\right]^2 \tag{B.6}$$

where $x_{ij}^{\alpha} = R_{ij}^{\alpha}/R_{ij}$, R_{ij}^{α} is the α component of the vector R_{ij}, and

$$\rho_j^{a(l)} = \exp\left[\beta_i^l \left(\frac{R_{ij}}{R_i^0} - 1\right)\right], \tag{B.7}$$

where β_i and R_i^0 are material dependent parameters.

Back to the embedding function:

$$F_i(\rho) = A_i E_i^0 \rho \ln \rho \tag{B.8}$$

where A_i is a constant to be determined and E_i^0 is the sublimination energy.

The pair interaction is given by:

$$\phi_{ii}(R) = \frac{2}{Z_i}\left[E_i^u(R) - F_i\left(\frac{\bar{\rho}_i^0(R)}{Z_i}\right)\right] \tag{B.9}$$

where Z_i is the number of nearest neighbors. The energy per atom of the reference structure is given by:

$$E_i^u(R) = -E_i^0(1 + a^*)e^{-a^*} \tag{B.10}$$

with:

$$a^* = \alpha_i \left(\frac{R}{R_i^0} - 1 \right) \tag{B.11}$$

and

$$\alpha_i^2 = \frac{9\Omega B}{E_i^0} \tag{B.12}$$

where B is the bulk modulus and Ω is the atomic volume of the solid element. In the end the potential requires 11 experimental constants.

Finally the screening function reduces the force between two atoms if a third atom is in the way (three-body interaction). And it is determined by the geometry of the lattice.

Appendix C

Numerical calculation of graphene's surface energy density Γ

The growth of a crack requires the creation of two new surfaces and hence an increase in the surface energy. As graphene is a two-dimensional sheet the new surfaces are actually edges and the surface energy is given by energy per length, and not the usual energy per area.

Numerically we can find the energy to create a new surface by simply separating the sheet from its fixed edges. This energy only depends on the interaction between atoms, obtained from the MEAM potential. Therefore here we do not apply a downward force, we do not have initial cracks, and no molecular dynamics is done. We start by fixing two sides of a graphene sheet. Then we move the rest of the sheet downward. Every time step the atoms are moved down by the same distance. The sheet moves farther and farther away from its fixed ends until finally the new surfaces are created, Fig. C.1. The surface energy Γ is then given by the change in energy divided by the length of the two edges created:

$$\Gamma_{numerical} = \frac{(E_{final} - E_{initial})}{2 \times \text{edge length}} \approx 3.82 \times 10^{-9}\text{J/m}. \tag{C.1}$$

This calculation does not substitute an experimental measurement of

the surface energy. It is fundamental to the theory of fracture that the surface energy be measured experimentally. We have not been able to find experimental values for this quantity in the literature.

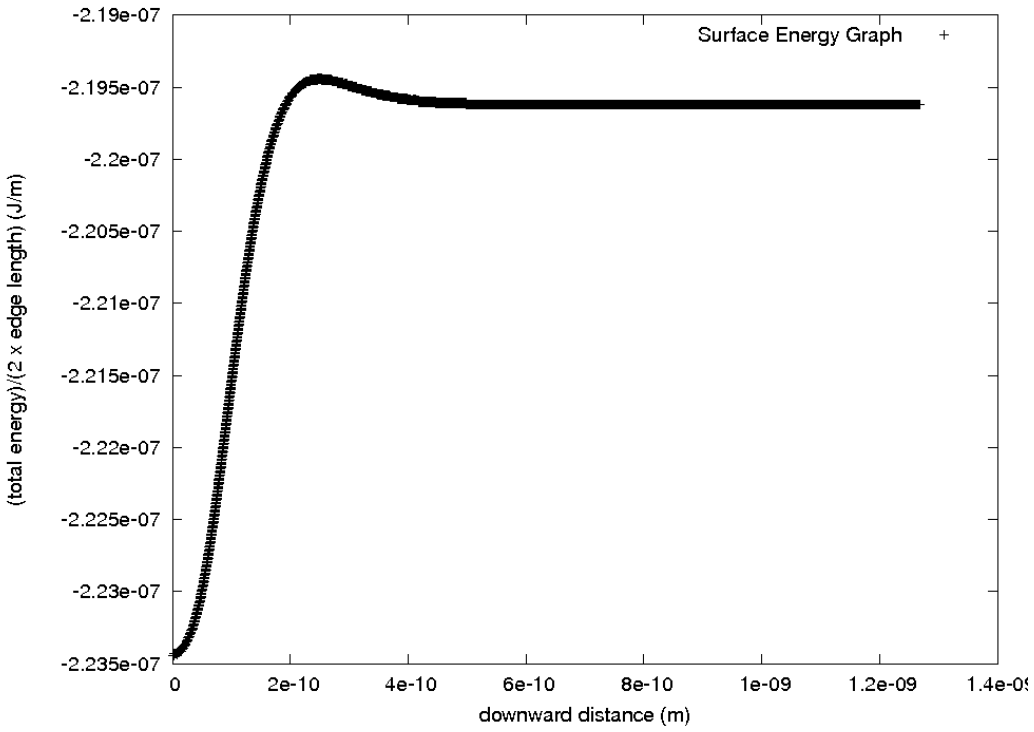

Figure C.1: Graph of energy per length (in Joules per meter) vs downward distance (in meters).

Appendix D

Movies of crack propagation

Below are links to movies we made on crack propagation. All movies are of a 100Å by 100Å clamped, free-standing graphene sheet under a constant downward force.

1. Edge crack

   Straight crack propagation: initial edge crack of $l \approx 10$Å and force of $f = 7.0 \times 10^{-11}$ N/atom:

   `http://youtu.be/Jx6yqbQTcGI`

   Non-straight crack propagation: initial edge crack of $l \approx 25$Å and force of $f = 2.8 \times 10^{-11}$ N/atom:

   `http://youtu.be/-KpUNZaA8yU`

   Top view: initial edge crack of $l \approx 30$Å and force of $f = 2.2 \times 10^{-11}$ N/atom:

   `http://youtu.be/v0QwP7yKN_s`

2. Crack in the middle of the sheet generated by defects

   Straight crack propagation: initial crack of $l \approx 15$Å in length and ≈ 2Å in width and force of $f = 4.5 \times 10^{-11}$ N/atom:

http://youtu.be/wYKQe0LhGHo

3. Crack in the middle of the sheet generated by a wide opening

   Straight crack propagation: initial crack of $l \approx 15$Å generated by an opening of $\approx 15^{\circ}$ and force of $f = 3.0 \times 10^{-11}$ N/atom:

   http://youtu.be/Dn4be5uOAfI

Appendix E

Table of numerical results

Table E.1: Table of minimum downward force for an initial crack to run on a 100Å by 100Å graphene sheet.

initial crack length (Å)	**edge crack (Newton/atom)**	**defect in the middle of the sheet (Newton/atom)**	**wide opening in the middle of the sheet (Newton/atom)**
10	7.0×10^{-11}	4.00×10^{-11}	3.90×10^{-11}
15	4.5×10^{-11}	3.00×10^{-11}	2.80×10^{-11}
20	3.5×10^{-11}	2.625×10^{-11}	2.50×10^{-11}
25	2.8×10^{-11}	2.27×10^{-11}	2.10×10^{-11}
30	2.2×10^{-11}	2.10×10^{-11}	1.85×10^{-11}
35	2.0×10^{-11}	1.875×10^{-11}	1.75×10^{-11}
40		1.75×10^{-11}	1.65×10^{-11}
45			1.55×10^{-11}
50			1.45×10^{-11}
55			1.35×10^{-11}
60			1.275×10^{-11}
65			1.20×10^{-11}
70			1.10×10^{-11}
75			0.95×10^{-11}
80			0.90×10^{-11}
85			0.80×10^{-11}

Bibliography

[1] *Private communication with Andre Geim.*

[2] *Private communication with Goldberg/Swan graphene group.*

[3] *Private communication with Insun Jo.*

[4] *Private communication with Jannik Meyer.*

[5] *Private communication with Kirill Bolotin.*

[6] *Private communication with Rodney S. Ruoff.*

[7] *Private communication with Rui Huang.*

[8] N. Abedpour, M. Neek-Amal, Reza Asgari, F. Shahbazi, N. Nafari, and M. Reza Rahimi Tabar. Roughness of undoped graphene and its short-range induced gauge field. *Physical Review B*, 76(19):195407, November 2007.

[9] M. I. Baskes. Modified embedded-atom potentials for cubic materials and impurities. *Physical Review B*, 46(5):2727–2742, 1992.

[10] M I Baskes, J E Angelo, and C L Bisson. Atomistic calculations of composite interfaces. *Modelling and Simulation in Materials Science and Engineering*, 2(3A):505–518, May 1994.

[11] Claire Berger, Zhimin Song, Xuebin Li, Xiaosong Wu, Nate Brown, Ccile Naud, Didier Mayou, Tianbo Li, Joanna Hass, Alexei N. Marchenkov, Edward H. Conrad, Phillip N. First, and Walt A. de Heer. Electronic confinement and coherence in patterned epitaxial graphene. *Science*, 312(5777):1191 –1196, May 2006.

[12] K. I. Bolotin, K. J. Sikes, J. Hone, H. L. Stormer, and P. Kim. Temperature-Dependent transport in suspended graphene. *Physical Review Letters*, 101(9):096802, 2008.

[13] K.I. Bolotin, K.J. Sikes, Z. Jiang, M. Klima, G. Fudenberg, J. Hone, P. Kim, and H.L. Stormer. Ultrahigh electron mobility in suspended graphene. *Solid State Communications*, 146(910):351–355, June 2008.

[14] Donald W. Brenner. Empirical potential for hydrocarbons for use in simulating the chemical vapor deposition of diamond films. *Physical Review B*, 42(15):9458–9471, November 1990.

[15] Johan M. Carlsson. Graphene: Buckle or break. *Nature Materials*, 6(11):801–802, November 2007.

[16] M. S Dresselhaus and G. Dresselhaus. Intercalation compounds of graphite. *ChemInform*, 33(51):228–228, December 2002.

[17] T.J. Echtermeyer, M.C. Lemme, M. Baus, B.N. Szafranek, A.K. Geim, and H. Kurz. Nonvolatile switching in graphene Field-Effect devices. *Electron Device Letters, IEEE*, 29(8):952 –954, August 2008.

[18] M. Eizenberg and J.M. Blakely. Carbon monolayer phase condensation on ni(111). *Surface Science*, 82(1):228–236, March 1979.

[19] A. Fasolino, J. H. Los, and M. I. Katsnelson. Intrinsic ripples in graphene. *Nature Materials*, 6(11):858–861, September 2007.

[20] I. Forbeaux, J.-M. Themlin, and J.-M. Debever. Heteroepitaxial graphite on 6H-SiC(0001): interface formation through conduction-band electronic structure. *Physical Review B*, 58(24):16396, December 1998.

[21] N. Garcia. Are graphene sheets stable? *cond-mat/0703515*, March 2007.

[22] D. Garcia-Sanchez, A. M. van der Zande, A. San Paulo, B. Lassagne, P. L. McEuen, and A. Bachtold. Imaging mechanical vibrations in suspended graphene sheets. *Nano Lett.*, 8(5):1399–1403, 2008.

[23] A. K. Geim and K. S. Novoselov. The rise of graphene. *Nat Mater*, 6(3):183–191, March 2007.

[24] M. Haluka, D. Obergfell, J. C Meyer, G. Scalia, G. Ulbricht, B. Krauss, D. H Chae, T. Lohmann, M. Lebert, M. Kaempgen, M. Hulman, J. Smet, S. Roth, and K. von Klitzing. Investigation of the shift of raman modes of graphene flakes. *physica status solidi (b)*, 244(11):4143–4146, November 2007.

[25] Dominic Holland and Michael Marder. Cracks and atoms. *Advanced Materials*, 11(10):793–806, July 1999.

[26] Masa Ishigami, J. H. Chen, W. G. Cullen, M. S. Fuhrer, and E. D. Williams. Atomic structure of graphene on SiO2. *Nano Lett.*, 7(6):1643–1648, 2007.

[27] Takazumi Kawai, Susumu Okada, Yoshiyuki Miyamoto, and Hidefumi Hiura. Self-redirection of tearing edges in graphene: Tight-binding molecular dynamics simulations. *Physical Review B*, 80(3):033401, July 2009.

[28] Roopam Khare, Steven L. Mielke, Jeffrey T. Paci, Sulin Zhang, Roberto Ballarini, George C. Schatz, and Ted Belytschko. Coupled quantum mechanical/molecular mechanical modeling of the fracture of defective carbon nanotubes and graphene sheets. *Physical Review B*, 75(7):075412, February 2007.

[29] Eun-Ah Kim and A. H. Castro Neto. Graphene as an electronic membrane. *EPL (Europhysics Letters)*, 84(5):57007, December 2008.

[30] Kwanpyo Kim, Vasilii I. Artyukhov, William Regan, Yuanyue Liu, M. F. Crommie, Boris I. Yakobson, and A. Zettl. Ripping graphene: Preferred directions. *Nano Lett.*, 12(1):293–297, 2011.

[31] T.A. Land, T. Michely, R.J. Behm, J.C. Hemminger, and G. Comsa. STM investigation of single layer graphite structures produced on pt(111) by hydrocarbon decomposition. *Surface Science*, 264(3):261–270, March 1992.

[32] L D Landau and E.M. Lifshitz. *Statistical Physics, Third Edition, Part 1: Volume 5*. Butterworth-Heinemann, 3 edition, January 1980.

[33] J. M. D. Lane and M. Marder. Numerical method for shock front hugoniot states. *AIP Conf. Proc*, 2006.

[34] Pierre Le Doussal and Leo Radzihovsky. Self-consistent theory of polymerized membranes. *Physical Review Letters*, 69(8):1209–1212, 1992.

[35] Byeong-Joo Lee and Jin Wook Lee. A modified embedded atom method interatomic potential for carbon. *Calphad*, 29(1):7–16, March 2005.

[36] Xuesong Li, Weiwei Cai, Jinho An, Seyoung Kim, Junghyo Nah, Dongxing Yang, Richard Piner, Aruna Velamakanni, Inhwa Jung, Emanuel Tutuc, Sanjay K. Banerjee, Luigi Colombo, and Rodney S. Ruoff. Large-Area synthesis of High-Quality and uniform graphene films on copper foils. *Science*, 324(5932):1312–1314, June 2009.

[37] Qiang Lu, Wei Gao, and Rui Huang. Atomistic simulation and continuum modeling of graphene nanoribbons under uniaxial tension. *Modelling and Simulation in Materials Science and Engineering*, 19(5):054006, July 2011.

[38] Qiang Lu and Rui Huang. Effect of edge structures on elastic modulus and fracture of graphene nanoribbons under uniaxial tension. *arXiv:1007.3298*, July 2010.

[39] Xuekun Lu, Hui Huang, Nikolay Nemchuk, and Rodney S. Ruoff. Patterning of highly oriented pyrolytic graphite by oxygen plasma etching. *Applied Physics Letters*, 75(2):193, 1999.

[40] Xuekun Lu, Minfeng Yu, Hui Huang, and Rodney S Ruoff. Tailoring graphite with the goal of achieving single sheets. *Nanotechnology*, 10(3):269–272, September 1999.

[41] M. Marder. Effects of atoms on brittle fracture. *International Journal of Fracture*, 130(2):517–555, November 2004.

[42] Michael P. Marder. *Condensed Matter Physics*. Wiley, 2 edition, November 2010.

[43] N. D. Mermin. Crystalline order in two dimensions. *Physical Review*, 176(1):250–254, December 1968.

[44] N. D. Mermin and H. Wagner. Absence of ferromagnetism or antiferromagnetism in one- or Two-Dimensional isotropic heisenberg models. *Physical Review Letters*, 17(22):1133–1136, November 1966.

[45] Jannik C. Meyer, A. K. Geim, M. I. Katsnelson, K. S. Novoselov, T. J. Booth, and S. Roth. The structure of suspended graphene sheets. *Nature*, 446(7131):60–63, March 2007.

[46] M. Marder M.J.B. Moura. Tearing Graphene. In ISBN: 978-1-4398-7142-3 TechConnect World, editor, *Nanotech 2011*, volume 1, pages 200–202, 15 June 2011.

[47] J. Moser, A. Verdaguer, D. Jimnez, A. Barreiro, and A. Bachtold. The environment of graphene probed by electrostatic force microscopy. *Applied Physics Letters*, 92(12):123507–123507–3, March 2008.

[48] Cherry A. Murray and David G. Grier. VIDEO MICROSCOPY OF MONODISPERSE COLLOIDAL SYSTEMS. *Annual Review of Physical Chemistry*, 47(1):421–462, October 1996.

[49] Ayato Nagashima, Kenji Nuka, Hiroshi Itoh, Takeo Ichinokawa, Chuhei Oshima, and Shigeki Otani. Electronic states of monolayer graphite formed on TiC(111) surface. *Surface Science*, 291(1-2):93–98, July 1993.

[50] David Nelson, Steven Weinberg, and T. Piran. *Statistical Mechanics of Membranes and Surfaces*. Wspc, 2 edition, June 2004.

[51] D.R. Nelson and L. Peliti. Fluctuations in membranes with crystalline and hexatic order. *Journal de Physique*, 48(7):8, 1987.

[52] R. Nicklow, N. Wakabayashi, and H. G. Smith. Lattice dynamics of pyrolytic graphite. *Physical Review B*, 5(12):4951, June 1972.

[53] K. S. Novoselov, A. K. Geim, S. V. Morozov, D. Jiang, Y. Zhang, S. V. Dubonos, I. V. Grigorieva, and A. A. Firsov. Electric field effect in atomically thin carbon films. *Science*, 306(5696):666 –669, October 2004.

[54] K. S. Novoselov, D. Jiang, F. Schedin, T. J. Booth, V. V. Khotkevich, S. V. Morozov, and A. K. Geim. Two-dimensional atomic crystals.

Proceedings of the National Academy of Sciences of the United States of America, 102(30):10451 –10453, July 2005.

[55] Taisuke Ohta, Aaron Bostwick, Thomas Seyller, Karsten Horn, and Eli Rotenberg. Controlling the electronic structure of bilayer graphene. *Science*, 313(5789):951 –954, 2006.

[56] V. N. Popov, V. E. Van Doren, and M. Balkanski. Elastic properties of single-walled carbon nanotubes. *Physical Review B*, 61(4):3078–3084, January 2000.

[57] Dipanjan Sen, Kostya S Novoselov, Pedro M Reis, and Markus J Buehler. Thin films: Small 10/2010. *Small*, 6(10):n/a–n/a, May 2010.

[58] V. B. Shenoy, C. D. Reddy, A. Ramasubramaniam, and Y. W. Zhang. Edge-Stress-Induced warping of graphene sheets and nanoribbons. *Physical Review Letters*, 101(24):245501, December 2008.

[59] Sasha Stankovich, Dmitriy A. Dikin, Geoffrey H. B. Dommett, Kevin M. Kohlhaas, Eric J. Zimney, Eric A. Stach, Richard D. Piner, SonBinh T. Nguyen, and Rodney S. Ruoff. Graphene-based composite materials. *Nature*, 442(7100):282–286, July 2006.

[60] Sasha Stankovich, Richard D. Piner, Xinqi Chen, Nianqiang Wu, SonBinh T. Nguyen, and Rodney S. Ruoff. Stable aqueous dispersions of graphitic nanoplatelets via the reduction of exfoliated graphite oxide in

the presence of poly(sodium 4-styrenesulfonate). *Journal of Materials Chemistry*, 16(2):155, 2006.

[61] Elena Stolyarova, Kwang Taeg Rim, Sunmin Ryu, Janina Maultzsch, Philip Kim, Louis E. Brus, Tony F. Heinz, Mark S. Hybertsen, and George W. Flynn. High-Resolution scanning tunneling microscopy imaging of mesoscopic graphene sheets on an insulating surface. *Proceedings of the National Academy of Sciences*, 104(22):9209–9212, May 2007.

[62] Sachin S. Terdalkar, Shan Huang, Hongyan Yuan, Joseph J. Rencis, Ting Zhu, and Sulin Zhang. Nanoscale fracture in graphene. *Chemical Physics Letters*, 494(4-6):218–222, July 2010.

[63] J. Tersoff. Energies of fullerenes. *Physical Review B*, 46(23):15546–15549, December 1992.

[64] R. C. Thompson-Flagg, M. J. B. Moura, and M. Marder. Rippling of graphene. *EPL (Europhysics Letters)*, 85(4):46002, February 2009.

[65] A.J. Van Bommel, J.E. Crombeen, and A. Van Tooren. LEED and auger electron observations of the SiC(0001) surface. *Surface Science*, 48(2):463–472, March 1975.

[66] S. C. Xu, S. Irle, D. G. Musaev, and M. C. Lin. Quantum chemical study of the dissociative adsorption of OH and H2O on pristine and defective graphite (0001) surfaces: Reaction mechanisms and kinetics. *J. Phys. Chem. C*, 111(3):1355–1365, 2006.

[67] Arend M. van der Zande, Robert A. Barton, Jonathan S. Alden, Carlos S. Ruiz-Vargas, William S. Whitney, Phi H. Q. Pham, Jiwoong Park, Jeevak M. Parpia, Harold G. Craighead, and Paul L. McEuen. Large-Scale arrays of Single-Layer graphene resonators. *Nano Letters*, 10(12):4869–4873, December 2010.

[68] Yuanbo Zhang, Joshua P. Small, William V. Pontius, and Philip Kim. Fabrication and electric-field-dependent transport measurements of mesoscopic graphite devices. *Applied Physics Letters*, 86(7):073104, 2005.

Index

Abstract, vi
Acknowledgments, v
Appendices, 93

Bibliography, 113

Dedication, iv

Vita

Maria João Brito Moura was born in Rio de Janeiro, Brazil on 27 July 1979, the daughter of Edgar P. Moura and Cynthia G. do N. Brito. She received the Bachelor of Science degree in Physics from the Universidade Federal do Rio de Janeiro in 2002. In 2005 she received the Masters degree in Physics from the Universidade do Estado do Rio de Janeiro. She applied to the University of Texas at Austin for enrollment in their physics program. She was accepted and started graduate studies in August, 2005.

Permanent address: The University of Texas at Austin, Department
of Physics, 1 University Station C1600
Austin, Texas 78712

This dissertation was typeset with LaTeX[†] by the author.

[†]LaTeX is a document preparation system developed by Leslie Lamport as a special version of Donald Knuth's TeX Program.